Validation of σ_2R/TMEM97 as a neuropathic pain target: Specificity, human expression and mechanism of action.

Short Title: σ_2R/TMEM97 modulators relieve pain

Authors: Muhammad Saad Yousuf[1,3], James J. Sahn[2,3], Eric T. David[1], Stephanie Shiers[1], Danielle M. Royer[1], Chelsea D. Garcia[1], Jennifer Zhang[1], Veronica M. Hong[1], Ayesha Ahmad[1], Benedict J. Kolber[1], Daniel J Liebl[4], Stephen F. Martin[2,3#] and Theodore J. Price[1,3#]

[1]Center for Advanced Pain Studies and Department of Neuroscience, School of Behavioral and Brain Sciences, University of Texas at Dallas, Richardson, TX 75080
[2]Department of Chemistry, University of Texas at Austin, Austin, TX 78712
[3]NuvoNuro, Austin, TX 78712
[4]University of Miami School of Medicine, Miami, FL

[#] Corresponding authors

Theodore J. Price 800 W Campbell Rd BSB 14.102 Richardson TX 75080 972-883-4311 Theodore.price@utdallas.edu	Stephen F. Martin Welch Hall 5.416 105 E. 24th St. Stop A5300 Austin, Texas 78712-1224 512-471-3915 sfmartin@mail.utexas.edu

Word count:
Abstract: 214
Significance Statement: 112
Document: 7485
Number of Text Pages: 12
Number of Figures: 7 (Supplementary figures: 5)
Number of Tables: 2

Classification: Neuroscience, Pharmacology
Keywords: Sigma 2 receptor, σ2 receptor, TMEM97, pain, drug discovery, ISR, dorsal root ganglion

Author Contributions: MSY, JJS, BJK, SFM, TJP designed research project; MSY, ETD, SS, DMR, CDG, JZ, VMH, AA performed experiments and analyzed data; JJS, SFM designed and synthesized small molecule modulators; DJL designed and bred novel TMEM97KO transgenic mice. MSY, TJP wrote the paper.

Competing Interest Statement: The authors declare financial relationships. Drs. Martin and Sahn report being co-inventors on patents and pending patent applications related to work described in this article. MSY, JJS, SFM and TJP are co-founders of NuvoNuro, Inc.

Abstract

The Sigma 2 receptor (σ_2R) was described pharmacologically more than three decades ago, but its molecular identity remained obscure until recently when it was identified as transmembrane protein 97 (TMEM97). We and others have shown that σ_2R/TMEM97 ligands produce analgesia in mouse neuropathic pain models with a time course wherein analgesic onset is 24 hours following dosing. We sought to understand this unique anti-neuropathic pain effect by addressing two key questions: do these σ_2R/TMEM97 compounds act selectively via the receptor, and what is their downstream mechanism on nociceptive neurons. Using male and female conventional knockout (KO) mice for *Tmem97,* we find that a novel σ_2R/TMEM97 binding compound, FEM-1689, requires the presence of the gene to produce analgesia in the spared nerve injury model in mice. Using primary mouse dorsal root ganglion (DRG) neurons, we demonstrate that FEM-1689 inhibits the integrated stress response and promotes neurite outgrowth via a σ_2R/TMEM97-specific action. We extend the clinical translational value of these findings by showing that FEM-1689 reduces ISR and p-eIF2α levels in human sensory neurons and that it alleviates the pathogenic engagement of ISR by methylglyoxal. We also demonstrate that σ_2R/TMEM97 is expressed in human nociceptors and satellite glial cells. These results validate σ_2R/TMEM97 as a promising target for further development for the treatment of neuropathic pain.

Significance Statement

Neuropathic pain is a major medical problem that is poorly treated with existing therapeutics. Our findings demonstrate that σ_2R/TMEM97 targeting with modulators creates analgesia in a mouse model via a specific action on the receptor. We also identify a potential mechanism of action, ISR inhibition, that links the receptor to cellular signaling events that have preclinical and clinical validation for pain relief. Our work suggests that σ_2R/TMEM97 can be selectively engaged by specific small molecules to produce ISR inhibition in a subset of cells that are critical for neuropathic pain. σ_2R/TMEM97-targeted therapeutics thus have the potential to offer effective pain relief without the side effects associated with currently available neuropathic pain medicines.

Introduction

Neuropathic pain, which is caused by an injury or disease of the somatosensory nervous system, affects approximately 10% of the population and is the leading cause of high-impact chronic pain (1). Management of neuropathic pain is a major clinical challenge because available drugs not only have limited efficacy, but they also elicit serious side effects. There is a significant need for novel drugs that alleviate neuropathic pain through non-opioid and non-addicting mechanisms and have improved side effect profiles.

The sigma 2 receptor (σ_2R) was recently identified in 2017 as transmembrane protein 97 (TMEM97) (2). We discovered that several small molecules that bind selectively to σ_2R/TMEM97 produce strong and long-lasting anti-neuropathic pain effects from spared nerve injury (SNI) in mice (3), a finding that was independently replicated with structurally distinct molecules (4). Although the biological function of σ_2R/TMEM97 is not well understood, it is a transmembrane protein that is associated with the endoplasmic reticulum (ER) and plays a role in calcium signaling (5, 6) and cholesterol trafficking and homeostasis (7-11). 20(*S*)-Hydroxycholesterol was recently identified as an endogenous ligand for σ_2R/TMEM97 (12). The role of σ_2R/TMEM97 in disease pathology has been focused on cancer (13), but it is also implicated in neurodegenerative diseases including Alzheimer's disease (14-17) and Parkinson's disease (18). Pharmacological targeting of σ_2R/TMEM97 has neuroprotective effects in a number of models of neurodegenerative conditions, including traumatic brain injury (19), Huntington's disease (20), and retinal ganglion cell degeneration (21).

The mechanism by which modulation of σ_2R/TMEM97 alleviates neuropathic pain is not known. Given the localization of σ_2R/TMEM97 at the ER, the primary hypothesis tested in our work is whether σ_2R/TMEM97 targeting may reduce pain via interference with the integrated stress response (ISR), which includes ER stress. The ISR is an adaptive response to cellular stressors such as accumulation of misfolded proteins, amino acid and heme deprivation, and viral infection (22, 23). A canonical signaling event associated with the ISR is phosphorylation of eukaryotic initiation factor 2α (eIF2α) in response to cellular stress conveyed by four kinases: protein kinase R (PKR), PKR-like ER kinase (10), heme-regulated inhibitor (HRI), general control nonderepressible 2 (GCN2). These kinases phosphorylate eIF2α, in turn, inhibiting global protein synthesis and promoting the translation of mRNAs with upstream open reading frames (uORF) like activated transcription factor 4 (ATF4). We and others have previously demonstrated that the induction of the ISR is associated with neuropathic pain caused by traumatic nerve injury (24, 25), metabolic disorders (26-28), and autoimmune disorders (29-31).

Another key question is whether the analgesic effects of σ_2R/TMEM97 ligands is specifically due to their binding to σ_2R/TMEM97 because such compounds can also have substantial activity at the sigma 1 receptor (σ_1R), a receptor that also produces analgesia in animal models (32-35). We used a recently developed knockout mouse of the *Tmem97* gene, and a new small molecule, FEM-1689, that has improved selectivity for σ_2R/TMEM97 to test the hypothesis that σ_2R/TMEM97 is causatively linked to analgesia in mouse neuropathic pain models. Indeed, the analgesic effect of FEM-1689 in mouse neuropathic pain is completely absent in TMEM97KO mice. Our findings also show that FEM-1689 inhibits the ISR in a σ_2R/TMEM97-dependent fashion in mouse and human DRG neurons. This work provides a strong mechanistic case for targeting of σ_2R/TMEM97 as the basis of a new approach to treat neuropathic pain.

Results

TMEM97 mRNA is expressed in the human and mouse dorsal root ganglia

To assess whether σ_2R/TMEM97 is expressed in human nociceptors, we performed RNAscope *in situ* hybridization using human dorsal root ganglia (DRG) obtained from organ donors. We found that *TMEM97* is expressed in all classes of human sensory neurons including *SCN10A* (Nav1.8)-positive, putative nociceptors (**Fig 1A-C**). Approximately 70% of all neurons expressed *SCN10A* transcripts, and all neurons evaluated expressed *TMEM97* (**Fig 1C**). The average diameter of neurons expressing *TMEM97* was roughly 74 µm as compared to *SCN10A*-expressing nociceptors that are 48 µm (**Fig 1D**). Upon further investigation, we found that *FABP7*-positive satellite glial cells also expressed *TMEM97* (**Fig 1E**). We validated our findings that *TMEM97* is expressed across all neuronal subtypes in the human DRG concurrent with our previously published human DRG spatial RNA sequencing dataset (36). Mouse DRG neurons and satellite glial cells also express *Tmem97* mRNA (**Supp Fig 1A**) with a nearly identical pattern to what was seen in the human DRG. Moreover, previously published single-cell RNA sequencing data, from mice shows that *Tmem97* is expressed in all DRG neuronal subtypes including *Scn10a*-positive nociceptors, and *Nefh*-positive large diameter proprioceptors and low-threshold mechanoreceptors (**Supp Fig 1B**) (37).

Discovery of FEM-1689 as a potent σ_2R/TMEM97 binding ligand

Methanobenzazocines and norbenzomorphans represent two distinct chemotypes of biologically active ligands that bind selectively to σ_2R/TMEM97 (**Fig 2**) (38, 39). The first group comprises UKH-1114, which alleviates mechanical hypersensitivity in a mouse model of neuropathic pain (3) and reduces neuronal toxicity in a model of Huntington's disease (20). Based on the positive outcomes using UKH-1114 as a treatment in models of neuropathic pain, we modified its chemical structure and synthesized FEM-1689 (**Supp Fig 2**), which is a highly selective compound with improved pharmacokinetic and physicochemical properties (**Fig 3**). FEM-1689 is >100-fold more selective for σ_2R/TMEM97 than 40 CNS proteins except for σ_1R (19-fold) and norepinephrine transporter (NET; 37-fold) (**Supp Table 1**).

Analgesic effect of FEM-1689 in male and female mice requires an intact Tmem97 gene

An important unresolved issue is whether σ_2R/TMEM97 ligands promote analgesia specifically through action on σ_2R/TMEM97. To address this question, we used a global TMEM97-knockout (KO) mouse. Male and female TMEM97KO animals and their wild-type counterparts had similar von Frey, Hargreaves', and acetone responses suggesting that the loss of TMEM97 did not alter their baseline evoked mechanical, heat, and cold sensitivity (**Supp Fig 3**). We then examined whether TMEM97KO animals develop an enhanced or blunted mechanical neuropathic pain phenotype following spared nerve injury (SNI) (40) (**Fig 4A**). Male and female TMEM97KO and wild-type animals developed severe and prolonged mechanical hypersensitivity following SNI tested at days 7, 10, and 14 after nerve injury (**Fig 4B, C**). Animals were tested thirty days following nerve injury and were found to be still mechanically hypersensitive. Male and female wild-type and TMEM97KO animals were then treated with a single intravenous injection of FEM-1689 dosed at 10 mg/kg, a dose determined based on previous studies with another σ_2R/TMEM97 ligand, UKH-1114 (3). We then assessed TMEM97KO and wild-type evoked mechanical threshold daily for 7 days and found little to no change in either group for mechanical sensitivity after 10 mg/kg of FEM-1689 (**Fig 4D, E**). Animals were allowed to recover for two weeks before a second treatment with a higher 20 mg/kg dose of FEM-1689. We found that a higher dose of 20 mg/kg was effective at reversing mechanical hypersensitivity in both males and female wild-type mice for roughly 4 days. Notably, FEM-1689 failed to produce analgesia in TMEM97KO mice suggesting that FEM-1689's effects were dependent on TMEM97. The effect size measurements for FEM-1689 were quantified for males (**Fig 4F**) and females (**Fig 4G**).

FEM-1689 inhibits the ISR and promotes neurite outgrowth in a σ_2R/TMEM97-dependent fashion

We then sought to identify the mechanism by which FEM-1689 acts on sensory neurons through σ_2R/TMEM97. Prior work has identified a link between σ_2R/TMEM97 and cholesterol synthesis and trafficking, processes that are heavily regulated by 5' adenosine monophosphate-activated protein kinase (AMPK) and its substrate, acetyl-CoA carboxylase (41). AMPK agonists are also known to produce analgesia in mouse models (22, 42-45). We treated cultured mouse DRG neurons with FEM-1689 at concentrations covering a range (10, 100, and 1000 nM) consistent with target binding (Ki = 11 nM) over the course of 16 hours and found no change in p-ACC levels whereas A769662 (100 µM), a known AMPK activator, increased p-ACC levels in both wild-type and TMEM97KO neurons (**Supp Fig 4 A, B**).

We then tested the hypothesis that FEM-1689 treatment might inhibit the ISR. Multiple lines of evidence support this hypothesis: 1) σ_2R/TMEM97 and ISR transducers like protein kinase R-like ER kinase (PERK) are located on the ER membrane (39, 46); 2) a recent report on the effect of 20(S)-hydroxycholesterol on σ_2R/TMEM97 implicated the ER-golgi network (12); and 3) the ISR is engaged in trauma-induced and diabetic neuropathic pain conditions (25, 26). We cultured mouse DRG neurons from wild-type and TMEM97KO animals, treated them with FEM-1689 over 16 hours, and measured changes in the levels of p-eIF2α using immunohistochemistry (**Fig 5A, B**). Interestingly, basal levels of p-eIF2α were much lower in TMEM97KO neurons than their wild-type counterparts. P-eIF2α levels following ISRIB treatment in wild-type neurons were comparable to p-eIF2α immunoreactivity in vehicle and ISRIB treated TMEM97KO neurons (**Fig 5C**). FEM-1689 reduced p-eIF2α levels, as compared to vehicle-treated cells, in wild-type mouse DRG neurons but not in DRG neurons cultured from TMEM97KO animals (**Fig 5D, E**). We found that FEM-1689 at 100 nM inhibited the ISR to the same extent as ISRIB (200 nM), a well-known ISR inhibitor (**Fig 5D**) (47). We calculated the p-eIF2α IC_{50} of FEM-1689 to be 30 nM in wild-type mouse DRG neurons, which was very similar to the binding affinity of FEM-1689 to TMEM97 (K_i=11 nM). FEM-1689 did not reduce levels of BiP, a chaperone important for initiating ER stress and ISR, in either wild-type or TMEM97KO neurons (**Supp Fig 4C, D**). Sholl analysis of cultured DRG neurons showed that FEM-1689 promoted neurite outgrowth in wild-type neurons but not in TMEM97KO cells (**Fig 5F-K**). Notably, neurite outgrowth in vehicle-treated TMEM97KO neurons was more pronounced than vehicle-treated wild-type neurons – an observation that may be due to reduced ISR in TMEM97KO cells and hence, enhanced protein synthesis. These data suggest that σ_2R/TMEM97 is necessary for FEM-1689 to reduce ISR and promote neurite outgrowth.

Norbenzomorphan σ_2R/TMEM97 ligands SAS-0132 and DKR-1677 enhance the ISR

We then assessed whether other compounds that bind to σ_2R/TMEM97 inhibit the ISR and whether ISR inhibition is specific to σ_2R/TMEM97 modulators that promote analgesia. The norbenzomorphans FEM-1689, SAS-0132 and DKR-1677 and methanobenzacocines UKH-1114 represent two structurally distinct chemotypes that interact with the binding site of σ_2R/TMEM97 in different orientations (39). SAS-0132 was previously shown to inhibit the analgesic effects of UKH-1114, which is a homolog of FEM-1689, suggesting that these two classes of molecules may exert opposing effects on σ_2R/TMEM97 biology. After treatment of wild-type mouse DRG neurons with 10, 30, 100, and 300 nM of SAS-0132 and DKR-1677 over 16 hours, we found that both compounds promoted the phosphorylation of eIF2α, in contrast to the inhibitory effects of FEM-1689 (Fig 6).

FEM-1689 inhibits the ISR in HEK293T cells

Human embryonic kidney (HEK) 293T cells express σ_2R/TMEM97 (The Human Protein Atlas (48)), so we queried whether FEM-1689 would inhibit ISR in this cell line. We demonstrate a concentration-dependent reduction in p-eIF2α immunoreactivity following FEM-1689 treatment using immunocytochemistry (ICC) and spectrophotometry (**Supp Fig 5A, B**). We tested the effect of FEM-1689 over nine concentrations, ranging from 0.1 nM to 1000 nM and measured the p-eIF2α IC_{50} of FEM-1689 in HEK cells to be 0.9 nM (**Supp Fig 5B**). We further examined a broader panel of ISR-related proteins with increasing concentrations of FEM-1689 using Western blotting. HEK293T cells treated with FEM-1689 over 16 hours showed a concentration-dependent reduction in phosphorylation of eIF2α, eIF2A, and p-PERK, while BiP expression remained relatively stable throughout (**Supp Fig 5C-K**).

FEM-1689 reduces p-eIF2α and reverses MGO-induced ISR activity in human sensory neurons

To extend and translate our rodent findings to humans, we treated cultured human sensory neurons from organ donors with FEM-1689 for 16 hours. Consistent with our mouse data, we discovered that FEM-1689 significantly reduced p-eIF2α levels in human neurons at concentrations of 10 and 100 nM (**Fig 7A, B**). We then assessed the potential of FEM-1689 to reverse pathological ISR activation in human cells. To induce ISR in vitro, we treated human sensory neurons with methylglyoxal (MGO, 1 μM) – a metabolic by-product of glycolysis that is implicated in diabetic neuropathic pain and other painful neurodegenerative disorders. We have previously demonstrated that MGO induces an ISR response that causes mechanical hypersensitivity in rodents (26). MGO treatment increased p-eIF2α levels in human DRG neurons and co-treatment with FEM-1689 (100 nM) prevented the increase in p-eIF2α levels (**Fig 7C, D**). These findings support the conclusion that ISR activation associated with stimuli that cause neuropathic pain in humans can be blocked by TMEM97 modulation.

Discussion

Our experiments clearly demonstrate that the analgesic effects of a σ_2R/TMEM97 ligand in mice of both sexes require direct modulation of σ_2R/TMEM97, not σ_1R or any other protein or receptor. This work also shows that modulation of σ_2R/TMEM97 leads to ISR inhibition in mouse and human neurons. Insofar as a reduction in ISR has previously been linked to pain relief (22, 26, 29), we believe it is a plausible cellular mechanism for the analgesia that is caused by FEM-1689. Finally, we show that human nociceptors express the *TMEM97* gene, FEM-1689 reduces eIF2α phosphorylation in cultured human sensory neurons and that the MGO-induced ISR in human sensory neurons can be reversed using FEM-1689. These observations suggest that targeting TMEM97 in pain patients could produce analgesia by inhibiting the ISR, a mechanism similarly observed in mice. We conclude that these findings validate σ_2R/TMEM97 as a *bona fide* target for neuropathic pain development.

The time course of action of σ_2R/TMEM97 modulators in mouse neuropathic pain models is different from many other analgesic compounds that have a rapid onset of action in accordance with the pharmacokinetics of the compound. Prior to this work, the slow onset time course of these analgesic effects in the mouse SNI model were independently observed by two different groups using distinct classes of σ_2R/TMEM97 ligands (3, 4). Here, we have shown that this effect is mediated specifically by σ_2R/TMEM97 because the antinociceptive activity is completely lost in male and female *Tmem97* knockout mice. These observations suggest that the kinetics of signaling for σ_2R/TMEM97 may be the primary underlying reason for the delayed analgesic response. The ISR is a major mechanism that controls long-lasting transcriptional changes by influencing the translation of key injury-induced transcription factors like activating transcription factor 4 (ATF4) and C/EBP homologous protein (CHOP). ISR mediated changes involving multiple transcriptional and post-translational modifications take time to initiate and

progress. It is possible that this time course is responsible for the delay in the temporal action of FEM-1689 versus the pharmacodynamics of ligand binding to σ_2R/TMEM97. The molecular signaling pathway downstream of σ_2R/TMEM97 activation requires further investigation.

Over the course of our studies to discover compounds that bind selectively to σ_2R/TMEM97, we have discovered several chemotypes that exhibit beneficial effects in a number of animal models (39). One group comprises aryl-substituted methanobenzazocines such as UKH-1114 and JVW-1034 (**Fig 2**). UKH-1114 alleviates mechanical hypersensitivity following nerve injury (3), and it reduces neuronal toxicity induced by mutant huntingtin protein in a model of Huntington's disease (20). The methanobenzazocine JVW-1034 not only reduces withdrawal behaviors in two rodent models of alcohol-dependence (49, 50), but it also alleviates heightened pain sensitivity that is induced by chronic alcohol exposure in mice (50). Herein we report that FEM-1689, a close analog of UKH-1114, also alleviates mechanical hypersensitivity following nerve injury. Another structural class of σ_2R/TMEM97 modulators include piperazine-substituted norbenzomorphans such as SAS-0132 and DKR-1677 (**Fig 2**). For example, SAS-0132 is neuroprotective and improves cognitive performance in animal models of age-related neurodegeneration (17, 51). Notably, SAS-0132 also blocks the antinociceptive activity of UKH-1114 (3), suggesting different σ_2R/TMEM97 binding compounds may have opposing effects on analgesia. DKR-1677, a homolog of SAS-0132, is protective in two different models of traumatic brain injury (TBI). It reduces axonal degeneration and provides dose-dependent enhancement of cognitive performance in the blast injury model of TBI, while it protects oligodendrocytes and cortical neurons in the controlled cortical impact model (19). DKR-1677 also protects retinal ganglion cells from ischemia/reperfusion injury (21). We demonstrate herein that SAS-0132 and DKR-1677 increase p-eIF2α expression in mouse DRG neurons and have the opposite effect on ISR as compared to FEM-1689. This observation is further substantiated by the observation that A011, an unrelated σ_2R/TMEM97 ligand, enhances ISR and promotes apoptosis in MCF-7 cells (52). These data show that σ_2R/TMEM97 modulators can have opposing effects on ISR and that a reduction in ISR via modulation of σ_2R/TMEM97 provides a screening framework for drug discovery for novel analgesics targeting this receptor.

Understanding how σ_2R/TMEM97 modulators affect the ISR requires further investigation, but there are various clues for direct and indirect influence on the ISR in the literature. Firstly, σ_2R/TMEM97 localization to the ER membrane may link it to the ISR via ER stress, particularly by influencing eIF2α phosphorylation by the kinase PERK. Indeed, we observed a reduction in p-PERK in HEK cells following FEM-1689 treatment at concentrations where p-eIF2α and eIF2A are maximally reduced (**Supp Fig 5**), suggesting a possible link between σ_2R/TMEM97 and PERK. Second, σ_2R/TMEM97 is likely involved in transporting bioactive lipids, such as hydroxycholesterols (12), between cellular compartments, perhaps via a transporter activity like that of Niemann-Pick C1 (NPC1) protein (9). Excessive lipid intake and the demand for increase lipid synthesis promote lipid stress of the ER that is known to activate the PERK-eIF2α branch of the ISR and impair mitochondrial function (53-55). Finally, σ_2R/TMEM97 regulates cellular Ca^{2+} dynamics via its influence on store-operated calcium entry (11). The ER is the largest Ca^{2+} store in the cell and is sensitive to fluctuations in Ca^{2+} levels causing ER stress and the ISR (56). It is currently unclear whether one or multiple mechanisms are required to produce analgesia associated with FEM-1689 and further investigation is required.

Neurite outgrowth can be used to assess the neuromodulatory, neuroprotective, and neuroregenerative effects of drugs (57). Our data demonstrate that FEM-1689 promotes neurite outgrowth and complexity in a σ_2R/TMEM97-dependent manner as measured by Sholl analysis. Neurons lacking σ_2R/TMEM97 have enhanced neurite outgrowth compared to their wild-type counterparts under naïve conditions. The reason for this may be due to a reduced ISR (**Fig 5C**),

and hence uninhibited protein synthesis in TMEM97KO neurons at basal levels. Neuroregeneration is a protein-demanding process, and drugs that inhibit ISR, like ISRIB, and thereby promote protein synthesis also enhance neurite outgrowth (58). TMEM97KO neurons have reduced p-eIF2α levels at baseline, comparable to levels of p-eIF2α in ISRIB-treated wild-type neurons. ISRIB treatment of TMEM97KO neurons does not further reduce p-eIF2α levels. This may represent a physiological floor effect where the ISR is inhibited maximally in TMEM97KO cell without being cytotoxic.

Nerve injury and regeneration are inherently linked such that the mechanisms that govern neuropathic pain are inversely correlated with neuroregenerative processes. Various neuropathic pain models, like SNI, diabetic neuropathy, and chemotherapy-induced neuropathy are characterized by reduced intraepidermal nerve fiber density while reinnervation into the epidermis in these models can alleviate pain hypersensitivity (59). Of note however aberrant innervation of the skin can also promote pain hypersensitivity suggesting that neuroregeneration is a balancing act between protective and detrimental mechanisms. We propose that modulating σ_2R/TMEM97 promotes appropriate neurite regrowth and enhances protective, analgesic regenerative processes.

There are limitations to our work. First, we have not shown a definitive link between ISR activation and analgesia *in vivo* with FEM-1689. One possibility would be to evaluate neuropathic pain in *Eif2s1*-knockout mice. Such an experiment is complicated because loss of eIF2α, encoded by *Eif2s1*, or completely preventing the phosphorylation of eIF2α through a point mutation is lethal (60). Moreover, no specific antagonists of eIF2α have been described. The widely used classes of compounds that inhibit ISR are chemical chaperones, ISR kinase inhibitors, and eIF2B-stabilizers like ISRIB do not directly target eIF2α and are not appropriate tools to answer this question. Second, despite the strong connection we have shown between FEM-1689 and σ_2R/TMEM97 for SNI-induced mechanical hypersensitivity, we fail to see any change in the nerve injury phenotype in TMEM97KO mice. This may point to an “agonist-like” action of FEM-1689. That is, the TMEM97KO (a permanent “antagonist”) mice would be expected to show an increase in pain but all of the animals are at a floor after SNI and their mechanical thresholds are technically indistinguishable. Third, we have not determined whether the activity of FEM-1689 is due to a peripheral or central site of action. While our pharmacokinetic experiments show that the compound readily enters the brain (Fig 2), we have shown a clear action on the DRG. Future experiments will use a cell-specific TMEM97 knockout mouse under development to solve this important issue.

We have validated σ_2R/TMEM97 as a neuropathic pain target and identified FEM-1689 as a candidate molecule for optimization for further development. The recent report of the crystal structure of σ_2R/TMEM97 bound with several ligands will facilitate advancements in σ_2R/TMEM97 structure-affinity relationships that can be leveraged to help develop novel compounds having suitable pharmacodynamic and pharmacokinetic profiles required of a clinical candidate.

Methods

Animals

TMEM97KO mice were donated by Dr. Liebl (University of Miami, Mouse Resource & Research Centers MMRRC, Tmem97$^{tm1(KOMP)Vlcg}$, stock #050147-UCD) (21). These mice were back crossed with C57BL/6 mice obtained from Charles River. A colony of these animals were maintained at University of Texas at Dallas. Knockout and wild-type animals were obtained from the same colony. Genotyping was performed using PCR (WT: Fwd: CCAATCCTCTACACACTCCTGTT Rev: CTGGTGGCCGTCCCTATTT, Mutant: Fwd:

ACTTGCTTTAAAAAACCTCCCACA. Rev: TCCTTCCCTGTAACCCATTTCTGGC). Animals were maintained on a 12-hour light-dark cycles. Adult male and female mice at least 12-week-old were used throughout the experiment. All experiments were in accordance with the National Institutes of Health guidelines and the Animal Care and Use Committee at the University of Texas at Dallas (protocol # 14-04).

Spared nerve injury model of neuropathic pain

Spared nerve injury (SNI) was performed by exposing the sciatic nerve and transecting the peroneal and tibial branches of the nerve, leaving the sural branch intact. Cut nerves were ligated using 4-0 sutures (Kent Scientific #SUT-15-2) and the wound was closed using surgical staples. In sham animals, an incision was made to expose the nerves, but the nerves were not transected. SNI and sham surgeries were completed on the same day in a randomized order. SNI and sham data were obtained from two separate cohorts of nerve injury experiments. Animals were anesthetized with isoflurane/oxygen (50:50) mixture delivered through a nose cone. We ensured that pain reflexes were lost prior to the surgery. A 100 µL subcutaneous injection of 10% gentamicin (Sigma-Aldrich #G1272) was used to prevent infections. Animals were monitored daily and tested for mechanical sensitivity at days 7, 10, and 14 post-surgery. Behavioral testing was technically completed blinded to surgical treatment (SNI vs sham) although SNI animals often exhibit some cupping of the paw making a full blinding impossible.

FEM-1689 intravenous administration

FEM-1689 was diluted in 100% dimethyl sulfoxide (DMSO, Fisher #67-68-5) to a concentration of 200 mM and stored at -20°C. It was further diluted in sterile 0.9% saline. The lateral tail vein was injected at 10 mg/kg or 20 mg/kg in 5µL per gram of mouse (100 µL for a 20-gram mouse) using a Hamilton syringe and 27-gauge needle. Animals were anesthetized with isoflurane/oxygen (50:50) during the injection. For behavioral experiments, all animals were injected with FEM-1689.

Mouse pain behavior assays

Baseline testing was completed four days prior to SNI/sham surgery (**Fig 4**). Animals were habituated for at least an hour in their apparatus before being tested. Experimenters were blinded to genotype for all behavior assays. Following SNI, blinding to the injury was not possible because animals will SNI develop a “cupped” hind paw. Blinding to genotype was still maintained. Mechanical paw withdrawal thresholds in mice were assessed using the Simplified Up-Down (SUDO) method of von Frey filaments test (61). Von Frey filaments were obtained from Ugo Basile and were calibrated in the lab using a weigh scale (VWR, 314AC) to 0.01 grams. Lateral surface of the paws were tested at baseline and following SNI.

Cold allodynia was assessed using drops of acetone applied to the plantar surface of each paw. Pain-like behaviors (i.e. vigorous shaking and licking) were timed for up to 45 seconds. Each paw was tested three times and both paws were averaged.

Thermal latency was measured using a Hargreaves device (62) (IITC Model 400, Life Science Inc.; Harvard Apparatus, CA) with the heated glass set at 29 °C, 40% active laser power, and a 20-second cutoff. Each paw was tested three times and both paws were averaged. Light was targeted to the lateral surface of the paws.

Mouse RNAscope in situ hybridization

A dorsal root ganglion (DRG) tissue (bilateral L1-L5) was collected from 10-week-old male C57BL6/J wild-type (WT) and littermate-matched TMEM97KO mice. The tissue was embedded in optimal cutting temperature (OCT, TissueTek) and was immediately flash-frozen in dry ice. The DRG were sectioned at 20 microns on a cryostat, and directly mounted onto Super Frost Plus charged slides. Slides were dried at –20 °C for 2 hours to increase tissue adherence and stored at –80 °C until used for RNAscope in situ hybridization.

RNAscope fluorescent in situ hybridization multiplex assay v2 was used as instructed by Advanced Cell Diagnostics (ACDBio Inc). Probes for *Tmem97* (ACD #527591), *Scn10a* [a marker for Nav1.8-expressing nociceptors] (ACD #426011), and *Fabp7* [a marker for satellite glial cells] (ACD #414651) were used to validate the deletion of *Tmem97* expression in TMEM97KO DRGs, and localization of *Tmem97* expression in WT DRGs. Every cohort of slides included at least one slide for negative control with no target probe (ACD #320871) and one positive control slide with three positive control target probe cocktails (ACD #320861) (62) for tissue quality check. Slides were removed from –80 °C and immediately immersed in pre-chilled (4 °C) 10% neutral buffer formalin for 15 min. The slides were rinsed twice in 1X phosphate-buffered saline (PBS, pH 7.4) and dehydrated in a series of different ethanol concentrations of 50%, 70%, and 100% (twice) for 5 min each at room temperature. The hydrophobic barrier was drawn around the section using a hydrophobic pen (ImmEdge PAP pen, Vector Labs) after briefly air drying. Slides were incubated with 1:2 diluted hydrogen peroxide in distilled water for 10 min at room temperature and washed twice in distilled water. The protease IV was applied to each section and incubated for 5 min at room temperature. Slides were washed twice in 1X PBS and RNA scope was performed immediately. A mixture of probes - *Tmem97, Scn10a, and Fabp7* – was hybridized for 2 hours at 40 °C in a humidity control tray inside a HybEZ oven. Signals for all three channels were amplified using a series of AMPs, and a TSA-based fluorescent label was developed for each channel using Opal 520, 570, and 690 dyes (Akoya Bioscience) for each channel. Slides were cover-slipped with Vectashield anti-fade mounting medium with DAPI. Images were captured using an Olympus FV 3000 confocal microscope at 100X magnification and each image used the same acquisition parameters for WT, TMEM97KO, and negative control slides. Imaging was not completed blinded to genotype.

Human samples – DRG culturing

In collaboration with the Southwest Transplant Alliance, human dorsal root ganglia (DRG) were obtained from organ donors (Supp Table 2). Once extracted, DRGs were either frozen in pulverized dry-ice for RNAScope experiments or immersed in ice-cold N-methyl-D-glutamate-supplemented artificial cerebrospinal fluid (as per (63)) until enzymatic dissociation. Human DRGs were cleaned of any fatty tissue and cut into small 1-mm chunks. These chunks were immersed in 5 ml of pre-warmed enzyme solution (2 mg/mL STEMzyme I, 4 µg/mL DNAse I obtained from Worthington Biochemical #LS004107 and #LS002139) in Hanks' Balanced Salt Solution (HBSS) without calcium and magnesium (Gibco #14170161). Enzyme solution containing the tissue was immersed in a shaking water bath at 37 °C for 20 min followed by trituration with glass pipettes. This step was repeated 2 - 3 times until the tissue was homogenized. Afterwards, cells were passed through a 100 µm cell strainer and the flow-through containing the cells was gently layered onto 3 mL of 10% bovine serum albumin (BSA, BioPharm #71-040-002) in HBSS in a 15 ml falcon tube. This BSA gradient containing the cells was centrifuged at 900g for 5 min at room temperature. The pellet containing the cells was resuspended in BrainPhys media (STEMCell #05790) containing 2% SM1 (STEMCell #05711), 1% N2-A (STEMCell #07152), 1% Pen-Strep (ThermoFisher #15070063), and 1% GlutaMax (Gibco #35050061). Human DRG neurons were plated and grown on glass coverslips coated with poly-D-lysine (Sigma #P7405). Cultured DRG neurons were plated for 24 hours before

being treated. Methyglyoxal (Sigma-Aldrich #M0252) and FEM-1689 were serially diluted in media.

Human samples - RNAscope in situ hybridization

Fresh frozen human DRGs were embedded in optimal cutting temperature (OCT, TissueTek) and sectioned at 20-microns onto charged slides. RNAScope was performed using the multiplex version 2 kit as instructed by ACDBio and as previously described (64) with slight modifications. Slides were fixed in buffered 10% formalin and dehydrated in 50%, 75%, and 100% ethanol. A 20-second protease III treatment was used throughout the experiment. Fluorescein β, Cy3, and Cy5 Akoya dyes were used. The probes were: *TMEM97* (ACD #554471), *FABP7* (ACD #583891-C2), *SCN10A* (ACD #406291-C3). RNA quality was assessed for each tissue using a positive control cocktail (ACD #320861). A negative control probe (ACD #320871) was used to check for non-specific labeling. Images at 40X magnification were acquired on a FV3000 confocal microscope (Olympus) and analyzed using Olympus CellSens. Neuronal diameter was measured using the polyline tool and was drawn across the widest area of the neuronal soma. Lipofuscins were identified as dense bodies of autofluorescence and not analyzed. Only puncta distinct from lipofuscin were analyzed. A positive cell was deemed to have at least one mRNA punctum.

Immunocytochemistry (ICC)

The immunocytochemistry protocol was based on a previously published protocol (65). Primary human and mouse cultured cells as well as HEK cells were fixed with 10% formalin for 10 min, and then washed three times with PBS (1X). Cells were blocked with 10% normal goat serum (NGS) (66) in PBS-triton X (0.1%). Antibodies were diluted in an antibody solution (2% NGS and 2% BSA in PBS-triton X). The antibodies used were as follows: p-eIF2α (1:500, Cell Signaling #3398), BiP (1:1000, Cell Signaling #3177), p-ACC Ser79 (1:500, Cell Signaling #3661), β3 tubulin (1:1000, Sigma #T8578), peripherin (1:1000, EnCor Biotechnology #CPCA-Peri) and DAPI (1:10,000, Cayman Chemicals #14285). Antibodies were incubated at 4 degrees Celsius overnight. The primary antibodies were washed with PBS-tween 20 (0.05%) three times, 10 min each. The secondary antibody Alexa Fluor 488 or Alexa Fluor 555 (Life Technologies, 1:1000) were dissolved in 2% NGS, 2% BSA in PBS-triton X and incubated at room temperature for 1 hour. The secondary antibody was washed with PBS-tween 20 (0.5%) thrice. DAPI was dissolved in PBS and added to the cells for 10 min. It was washed with PBS twice. Each experiment had a primary omission control where the primary antibody was replaced with only the antibody solution to discern any nonspecific binding of the secondary antibody. Coverslips were mounted onto microscope slides and imaged on a confocal. Images were analyzed using Olympus CellSens. Neurons were preferentially selected by their presence of β3 tubulin. ROIs were set to cover the cell soma and mean gray intensities of each cell was measured.

HEK cells

Human embryonic kidney (HEK) 293T cells (ATCC # CRL-3216) were generously donated by the Campbell Lab (UT Dallas). Cell stocks were previously frozen at 1 million cells/ml in 90% fetal bovine serum (FBS, ThermoFisher #SH300880340) and 10% DMSO. Cells were grown in complete medium (10% FBS, 1% Pen-Strep in DMEM/F12 + GlutaMax (Gibco #10565-018) in T-75 flasks (Greiner Bio-One #658175). Cells were maintained at 37 °C with 5% CO_2 and passaged twice before being plated onto either 96-well or 6-well plates for ICC/spectrophotometry and western blotting, respectively. Cells were counted using the TC20 automated cell counter (Bio-Rad #1450102) using a 1:1 dilution of trypan blue (Gibco #15250061).

In a 96-well plate (ThermoFisher #165305), cells were plated at a density of 20,000 cells per well and grown to roughly 65% confluency before being treated with FEM-1689 overnight. Three replicates were made per condition/dose (1/2 log steps ranging from 0.1 nM to 1000 nM). HEK cells were fixed with buffered 10% formalin for 10 min and washed three times with 1X PBS. ICC was performed as outlined previously. Cells were stained for p-eIF2α and DAPI. Immunofluorescence of HEK cells was quantified using the Synergy HTX Multimode Reader. Two filters were used: excitation 360/40nm emission 460/40 (DAPI), and excitation 485/20nm emission 528/20 (p-eIF2α-AlexaFluor 488). Wells were topped with 100 µL of 1X PBS prior to being read. All reads were performed at bottom with a gain of 35. Area scans of 5x5 matrix was used with 497x497 micron point spacing. Negative control wells did not receive any primary antibody, but the remainder of the protocol was the same. Relative fluorescence units (RFUs) of the negative controls were subtracted from each well. P-eIF2α fluorescence was normalized to DAPI in order to control for the number of cells present in the well and then to the fluorescence of the vehicle treatment as a percentage. Values were plotted in a X-Y plot in GraphPad Prism. Concentrations were transformed to log2 values and data was fit to a non-linear regression curve (inhibitor vs response, variable slope, four parameters) constrained at top=100 and IC_{50}>0.

Western blotting

HEK cells were plated at 60,000 cells per well onto six-well plates (ThermoFisher # 351146) for 24 hours before being treated with FEM-1689 overnight. Protein extractions and western blotting was performed as previously published (29). In brief, media from the cells was removed and cells were washed once with 1X PBS. Cells were lysed in the well with radioimmunoprecipitation assay (RIPA) buffer consisting of 25 mM Tris, 150 mM NaCl, 0.1% SDS, 0.5% Na deoxycholate, 1% Triton X-100 with protease and phosphatase inhibitor cocktails (Sigma Aldrich P8340, P5726, P0044 – 1:100 each). Cells were centrifuged at 4 °C at 14,000 rpm for 10 min. The supernatant was used for downstream analysis. Protein was quantified using the Pierce BCA Protein Assay kit (Thermo Scientific, #23225) according to the manufacturer's instructions.

Protein samples were denatured using 4X Laemmli Sample buffer (BioRad #1610747) and heated at 95 °C for 5 min. 20 µg of protein samples were loaded onto 4-20% Stain-Free Criterion TGX gels (BioRad #5678094). Gels were run in Tris/Glycine/SDS running buffer (BioRad #1610772) at 120V for roughly 1.5 hours. Stain-Free gels were activated for 5 min prior to the transfer step. Protein was transferred for 10 min onto low fluorescence polyvinylidene difluoride (PVDF) using a TransBlot Transfer kit (BioRad #1704275) and a Transblot Turbo transfer system (BioRad). Once transferred, total protein was imaged immediately using a ChemiDoc MP system (BioRad). Blots were allowed to dry for 5 min and were blocked with 5% non-fat milk in Tris buffered saline (TBS)-Tween 20 (0.05%). Antibodies were diluted in 1% non-fat milk in TBS-Tween 20. Primary antibodies used in this study were: p-eIF2α (1:1000, Cell Signaling #3398), t-eIF2α (1:1000, Cell Signaling #9722), eIF2A (1:2500, Abcam #ab169528), p-PERK (1:500, Cell Signaling #3192), t-PERK (1:1000, Cell Signaling #3179), BiP (1:1000, Cell Signaling #3177). Goat anti-Rabbit IgG horseradish peroxidase (HRP) (H+L) (1:10,000) was used as a secondary antibody. Stained blots were imaged using enhanced chemiluminescence (ECL) on a ChemiDoc MP system.

Mouse DRG cultures

Mouse DRGs were harvested from naïve wild-type and TMEM97KO mice euthanized following isoflurane anesthesia and decapitated. Mouse DRGs were processed and plated as outlined in the human DRG section above with minor differences. Lumbar DRGs of two male and two female mice were cultured together and plated across 4 well replicates of each condition.

Mouse DRG neurons were grown in DMEM/F12+GlutaMax (Gibco #10565-018) plus 1% Pen-Strep and 1% N2-A. Cultured cells were plated on glass coverslips for 24 hours before being treated with FEM-1689. SAS-0132 and DKR-1677 were dissolved in 100% DMSO to a final concentration of 200mM and stored at -20 °C. FEM-1689, SAS-0132, and DKR-1677 were serially diluted in media. Untreated media was completely replaced with media containing each compound.

Neurite outgrowth and Sholl analysis

Cultured mouse DRG neurons from wild-type and TMEM97KO animals were treated with either vehicle or FEM-1689 (100 nM). These cells were immunolabeled with β3 tubulin and DAPI according to the ICC protocol detailed above. Cells were imaged at 20X magnification on a FV3000 confocal microscope (Olympus) and Z-stacked in 1 µm intervals. Images were compiled as maximum Z-stack on ImageJ and transformed to 8-bit images. Sholl analysis was performed using the Neuroanatomy plugin in ImageJ according to the authors recommendations (67). Only solitary cells were used for analysis. The output for each cell was the number of intersections in 1-micron increments. The number of intersections was averaged for each condition across all cells. The area under the curve was calculated using GraphPad Prism.

Synthetic procedures and characterization

Binding assays. Sigma receptor binding assays for FEM-1686, which was determined to be >95% pure (LC-MS), were performed by the National Institutes of Mental Health Psychoactive Drug Screening Program (NIMH PDSP) at Chapel Hill, North Carolina (68). σ_1R and σ_2R/TMEM97 were sourced from HEK293T cells transfected with human σ_1R and σ_2R/TMEM97. σ_1R binding affinity (K_i) was determined through competition binding assays with [^{3}H]-(+)-pentazocine, whereas σ_2R/TMEM97 binding affinity (K_i) was determined through competition binding assays using the radioligand [^{3}H]-ditolylguanidine in the presence of (+)-pentazocine to block σ_1R binding sites. K_i values are calculated from an average of two or more independent experiments. Detailed experimental protocols are available on the NIMH PDSP website at https://pdspdb.unc.edu/pdspWeb.

General. Commercial reagents and solvents were used without purification unless stated, but acetonitrile (MeCN) was dried by filtration through two columns of activated molecular sieves. Glassware was dried overnight in an oven at 120 °C or flame dried under vacuum for a minimum of 5 min. All air- or moisture-sensitive reactions were performed under an atmosphere of argon or nitrogen. Reaction temperatures refer to the temperature of the heating or cooling bath. Volatile solvents were removed under reduced pressure using a Büchi rotary evaporator at 25–30 °C. Air- or moisture-sensitive reagents and all solvents were transferred using plastic syringes and steel needles using standard techniques. Proton nuclear magnetic resonance (^{1}H NMR) and carbon nuclear magnetic resonance (^{13}C NMR) spectra were recorded at the indicated field strength in $CDCl_3$. Chemical shifts are reported in parts per million (δ) and are referenced to the deuterated solvent. Coupling constants (*J*) are reported in Hertz (69), and the splitting abbreviations used are: s, singlet; d, doublet; t, triplet; q, quartet; dt, doublet of triplets; ddd, doublet of doublets of doublets; m, multiplet; br s, broad singlet;. Capillary melting points are uncorrected. Accurate mass measurements were determined using an LC-MS system comprised of an Agilent 1260 series HPLC and an Agilent 6530 single quadrupole time-of-flight mass spectrometer. Purities of all compounds submitted for testing at PDSP were determined by LC-MS from the areas under the curves (AUC) at 214 and 254 nm. Column chromatography was performed using glass columns and “medium pressure” silica gel (Sorbent Technologies, 45-70 µ).

*Benzyl 8-(4-(trifluoromethyl)phenyl)-1,3,4,5-tetrahydro-2H-1,5-methanobenzo[c]azepine-2-carboxylate (**2**).* A solution of aryl chloride **1** (70) (327 mg, 1.0 2.0 mmol), 4-trifluoromethylphenylboronic acid (379 mg, 2.0 mmol), Cs_2CO_3 (650 mg, 2.0 mmol), palladium(bis)(*t*-butyl)$_3$ phosphine (25.5 mg, 0.05 mmol) in degassed 1,4-dioxane (4 mL) was stirred for 21 h at 100 °C. The reaction was cooled to room temperature and poured into water (5 mL). The mixture was extracted with CH_2Cl_2 (3 × 15 mL), and the combined organic layers were dried ($MgSO_4$) and concentrated under reduced pressure. The crude product was purified via flash column chromatography (SiO_2), eluting with hexane/EtOAc (50:1 to 20:1 to 13:1 v/v) to afford 367.2 mg (83%) of **2** as a pale yellow oil. ^{1}H NMR (500 MHz, as a mixture of rotamers) δ 7.72-7.24 (comp, 12 H), 5.61 (br s, 0.5 H), 5.49 (br s, 0.5 H), 5.27-5.07 (comp, 2 H), 3.96-3.81 (m, 1 H), 3.39-3.24 (m, 1 H), 2.61-2.43 (m, 1 H), 2.34-2.20 (m, 1 H), 2.12-2.00 (m, 1 H), 1.94 (d, *J* = 11.0 Hz, 1 H), 1.74-1.59 (m, 1 H). ^{13}C NMR (126 MHz, as a mixture of rotamers) δ 155.0, 154.8, 146.5, 144.6, 142.1, 141.9, 139.0, 136.9, 136.8, 129.2 (q, J_{C-F} = 31.5 Hz), 128.4, 127.9, 127.8, 127.3, 125.6 (q, J_{C-F} = 3.8 Hz), 123.3 (q, J_{C-F} = 272.2 Hz), 123.2, 122.7, 122.5, 67.0, 57.6, 57.3, 43.6, 39.5, 38.6, 30.2. HRMS (ESI) *m/z* calcd for $C_{26}H_{22}F_3NNaO_2$ $(M+Na)^+$, 460.1495; found 460.1499.

8-*(4-(Trifluoromethyl)phenyl)-2,3,4,5-tetrahydro-1H-1,5-methanobenzo[c]azepine (**3**).* A mixture of **2** (243 mg, 0.55 mmol), 10% Pd/C (85 mg) and EtOH (4 mL) was stirred under a H_2 balloon at room temperature for 5 h. The mixture was filtered through a pad of Celite, which was washed with CH_2Cl_2 (2 mL), and the combined filtrate and washings were concentrated under reduced pressure. The crude product was purified via flash column chromatography (SiO_2), eluting with MeOH/NEt_3/EtOAc (1:1:8), to afford 150 mg (90%) of **3** as a clear oil. ^{1}H NMR (500 MHz) δ 7.76 (s, 1 H), 7.68 (q, *J* = 8.5 Hz, 4 H), 7.56 (dd, *J* = 7.5, 1.5 Hz, 1 H), 7.34 (d, *J* = 8.0 Hz, 1 H), 7.11 (br s, 1 H), 4.67 (d, *J* = 2.5 Hz, 1 H), 3.38 (s, 1 H), 3.07 (dd, *J* = 13.0, 5.5 Hz, 1 H), 2.49 (td, *J* = 12.5, 5.0 Hz, 1 H), 2.42 – 2.33 (comp, 2 H), 2.22 (td, *J* = 12.5, 5.0 Hz, 1 H), 1.67 (d, *J* = 13.5 Hz, 1 H). ^{13}C NMR (126 MHz) δ 146.1, 144.2, 139.6, 139.1, 129.3 (q, J_{C-F} = 32.5 Hz), 128.6, 127.4, 125.7 (q, J_{C-F} = 3.8 Hz), 124.2 (q, J_{C-F} = 272.2 Hz), 123.2, 123.1, 58.0, 42.7, 38.8, 38.1, 28.3. HRMS (ESI) *m/z* calcd for $C_{18}H_{17}F_3N$ $(M+H)^+$, 304.1308; found 304.1309.

3-((1S,5R)-8-(4-(Trifluoromethyl)phenyl)-1,3,4,5-tetrahydro-2H-1,5-methanobenzo[c]azepin-2-yl)propan-1-ol (FEM-1689). To a solution of **3** (191.2 mg, 0.63 mmol) in acetonitrile (6 mL) was added K_2CO_3 (261.2 mg, 1.89 mmol), followed by 3-bromopropan-1-ol (175.2 mg, 1.26 mmol). The reaction mixture was heated to 60 °C for 21 h. The reaction mixture was cooled to room temperature and filtered, and the filtrate was concentrated under reduced pressure. The residue was suspended in 1 M aqueous HCl (5 mL) and washed with ether (5 mL). The aqueous phase was basified (pH ~ 8) with 2 M aqueous NaOH and extracted with CH_2Cl_2 (3 × 20 mL). The extracts were combined, dried (Na_2SO_4), filtered, and concentrated reduced pressure. The residue was purified by a column chromatography (SiO_2) using CH_2Cl_2:MeOH (30:1 to 15:1) as eluant to yield 115.8 mg (51%) FEM-1689 as a colorless oil.^{1}H NMR (500 MHz) δ 7.69 (s, 4 H), 7.49 (dd, *J* = 7.6, 1.7 Hz, 1 H), 7.39 (s, 1 H), 7.31 (d, *J* = 7.6 Hz, 1 H), 4.16 (d, *J* = 4.6 Hz, 1 H), 3.93 – 3.79 (comp, 2 H), 3.21 (br. s, 1 H), 2.84 (dd, *J* = 11.7, 5.7 Hz, 1 H), 2.77 (ddd, *J* = 12.0, 7.5, 3.8 Hz, 1 H), 2.39 (ddd, *J* = 12.2, 7.8, 3.8 Hz, 1 H), 2.32 – 2.26 (m, 1 H), 2.07 – 1.98 (m, 1 H), 1.97 (d, *J* = 11.0 Hz, 1 H), 1.86 – 1.76 (m, 1 H), 1.75 – 1.66 (m, 1 H), 1.61 – 1.55 (m, 1 H), 1.50 (td, *J* = 11.9, 4.8 Hz, 1 H). ^{13}C NMR (126 MHz) δ 146.9, 145.1, 139.5, 138.4, 129.30 (q, J_{C-F} = 32.4 Hz), 127.5, 127.4, 125.8 (q, J_{C-F} = 3.8 Hz), 124.6 (q, J_{C-F} = 272.4 Hz), 123.2, 123.1, 64.9, 63.6, 56.7, 47.1, 44.7, 39.7, 30.1, 27.2. HRMS (FIA) *m/z* calcd for $C_{21}H_{23}F_3NO$ $(M+H)^+$ 408.1934; found 408.1933.

Data Analysis

All results are presented at mean ± standard error of mean (SEM). Statistical differences between two groups were determined by two-tailed Student's t-test. One-way and two-way ANOVAs with repeated measures were used when comparing more than two conditions. Tukey's or Holm-Sidak's post hoc analysis was performed. Specific statistical tests are detailed in figure legends. Statistical significance was set at $p<0.05$. Data was analyzed and graphed on GraphPad Prism 9.5.1. BioRender was used to build experimental schematics. Effect sizes for FEM-1689 effects on mechanical sensitivity were calculated for each animal and averaged for the group. Effect size = |(baseline-baseline) + (baseline-day1) + ... + (baseline-day7)|.

Acknowledgements:
This work was supported by Postdoctoral Fellowship Program of Natural Sciences and Engineering Research Council of Canada and by NIH grant R01 NS0655926 (TJP). The authors are grateful to the organ donors and their families for the gift of life and research provided by their organ donation. The authors thank Anna Cervantes, Geoffrey Funk, and Peter Horton of the Southwest Transplant Alliance for human tissue recovery. We are grateful to the Robert A. Welch Foundation (F-0652) for funding. We also thank the UT Austin Mass Spectrometry Facility for high resolution mass spectral data and the NIH (Grant Number 1 S10 OD021508-01) for funding the Bruker AVANCE III 500 MHz spectrometer used to characterize new compounds. We are also grateful for the Ki determinations that were generously provided by the National Institute of Mental Health's Psychoactive Drug Screening Program, Contract # HHSN-271-2018-00023-C (NIMH PDSP). The NIMH PDSP is Directed by Professor Bryan L. at the University of North Carolina at Chapel Hill and Project Officer Jamie Driscoll at NIMH, Bethesda MD, USA.

References:

1. J. Dahlhamer *et al.*, Prevalence of Chronic Pain and High-Impact Chronic Pain Among Adults - United States, 2016. *MMWR Morb Mortal Wkly Rep* **67**, 1001-1006 (2018).
2. A. Alon *et al.*, Identification of the gene that codes for the sigma2 receptor. *Proc Natl Acad Sci U S A* **114**, 7160-7165 (2017).
3. J. J. Sahn, G. L. Mejia, P. R. Ray, S. F. Martin, T. J. Price, Sigma 2 Receptor/Tmem97 Agonists Produce Long Lasting Antineuropathic Pain Effects in Mice. *ACS Chem Neurosci* **8**, 1801-1811 (2017).
4. A. Alon *et al.*, Structures of the sigma2 receptor enable docking for bioactive ligand discovery. *Nature* **600**, 759-764 (2021).
5. G. Cassano *et al.*, F281, synthetic agonist of the sigma-2 receptor, induces Ca2+ efflux from the endoplasmic reticulum and mitochondria in SK-N-SH cells. *Cell Calcium* **45**, 340-345 (2009).
6. B. J. Vilner, W. D. Bowen, Modulation of Cellular Calcium by Sigma-2 Receptors: Release from Intracellular Stores in Human SK-N-SH Neuroblastoma Cells. *Journal of Pharmacology and Experimental Therapeutics* **292**, 900-911 (2000).
7. A. Riad *et al.*, The Sigma-2 Receptor/TMEM97, PGRMC1, and LDL Receptor Complex Are Responsible for the Cellular Uptake of Aβ42 and Its Protein Aggregates. *Molecular Neurobiology* **57**, 3803-3813 (2020).
8. A. Riad *et al.*, Sigma-2 Receptor/TMEM97 and PGRMC-1 Increase the Rate of Internalization of LDL by LDL Receptor through the Formation of a Ternary Complex. *Sci Rep* **8**, 16845 (2018).
9. D. Ebrahimi-Fakhari *et al.*, Reduction of TMEM97 increases NPC1 protein levels and restores cholesterol trafficking in Niemann-pick type C1 disease cells. *Hum Mol Genet* **25**, 3588-3599 (2016).

10. F. Bartz *et al.*, Identification of cholesterol-regulating genes by targeted RNAi screening. *Cell Metab* **10**, 63-75 (2009).
11. C. Cantonero, P. J. Camello, G. M. Salido, J. A. Rosado, P. C. Redondo, TMEM97 facilitates the activation of SOCE by downregulating the association of cholesterol to Orai1 in MDA-MB-231 cells. *Biochim Biophys Acta Mol Cell Biol Lipids* **1866**, 158906 (2021).
12. Y.-S. Cheng *et al.*, A proteome-wide map of 20(S)-hydroxycholesterol interactors in cell membranes. *Nature Chemical Biology* **17**, 1271-1280 (2021).
13. Y. S. Huang, H. L. Lu, L. J. Zhang, Z. Wu, Sigma-2 receptor ligands and their perspectives in cancer diagnosis and therapy. *Med Res Rev* **34**, 532-566 (2014).
14. M. Grundman *et al.*, A phase 1 clinical trial of the sigma-2 receptor complex allosteric antagonist CT1812, a novel therapeutic candidate for Alzheimer's disease. *Alzheimers Dement (N Y)* **5**, 20-26 (2019).
15. N. J. Izzo *et al.*, Alzheimer's Therapeutics Targeting Amyloid Beta 1–42 Oligomers I: Abeta 42 Oligomer Binding to Specific Neuronal Receptors Is Displaced by Drug Candidates That Improve Cognitive Deficits. *PLoS ONE* **9**, e111898 (2014).
16. N. J. Izzo *et al.*, Alzheimer's Therapeutics Targeting Amyloid Beta 1–42 Oligomers II: Sigma-2/PGRMC1 Receptors Mediate Abeta 42 Oligomer Binding and Synaptotoxicity. *PLoS ONE* **9**, e111899 (2014).
17. B. Yi *et al.*, Small molecule modulator of sigma 2 receptor is neuroprotective and reduces cognitive deficits and neuroinflammation in experimental models of Alzheimer's disease. *J Neurochem* **140**, 561-575 (2017).
18. C. S. Limegrover *et al.*, Sigma-2 receptor antagonists rescue neuronal dysfunction induced by Parkinson's patient brain-derived α-synuclein. *Journal of Neuroscience Research* **99**, 1161-1176 (2021).
19. E. Vazquez-Rosa *et al.*, Neuroprotective Efficacy of a Sigma 2 Receptor/TMEM97 Modulator (DKR-1677) after Traumatic Brain Injury. *ACS Chem Neurosci* **10**, 1595-1602 (2019).
20. J. Jin *et al.*, Neuroprotective Effects of σ_2R/TMEM97 Receptor Modulators in the Neuronal Model of Huntington's Disease. *ACS Chemical Neuroscience* **13**, 2852-2862 (2022).
21. H. Wang *et al.*, σ2R/TMEM97 in retinal ganglion cell degeneration. *Scientific Reports* **12** (2022).
22. M. S. Yousuf, S. I. Shiers, J. J. Sahn, T. J. Price, Pharmacological Manipulation of Translation as a Therapeutic Target for Chronic Pain. *Pharmacol Rev* **73**, 59-88 (2021).
23. K. Pakos-Zebrucka *et al.*, The integrated stress response. *EMBO Rep* **17**, 1374-1395 (2016).
24. E. Zhang *et al.*, Endoplasmic reticulum stress impairment in the spinal dorsal horn of a neuropathic pain model. *Scientific Reports* **5**, 11555 (2015).
25. O. K. Melemedjian *et al.*, Targeting adenosine monophosphate-activated protein kinase (AMPK) in preclinical models reveals a potential mechanism for the treatment of neuropathic pain. *Mol Pain* **7**, 70 (2011).
26. P. Barragan-Iglesias *et al.*, Activation of the integrated stress response in nociceptors drives methylglyoxal-induced pain. *Pain* **160**, 160-171 (2019).
27. B. Inceoglu *et al.*, Endoplasmic reticulum stress in the peripheral nervous system is a significant driver of neuropathic pain. *Proc Natl Acad Sci U S A* **112**, 9082-9087 (2015).
28. S. Lupachyk, P. Watcho, R. Stavniichuk, H. Shevalye, I. G. Obrosova, Endoplasmic reticulum stress plays a key role in the pathogenesis of diabetic peripheral neuropathy. *Diabetes* **62**, 944-952 (2013).

29. M. S. Yousuf *et al.*, Endoplasmic reticulum stress in the dorsal root ganglia regulates large-conductance potassium channels and contributes to pain in a model of multiple sclerosis. *FASEB J* **34**, 12577-12598 (2020).
30. S. Stone *et al.*, Activating transcription factor 6alpha deficiency exacerbates oligodendrocyte death and myelin damage in immune-mediated demyelinating diseases. *Glia* **66**, 1331-1345 (2018).
31. S. Stone, W. Lin, The unfolded protein response in multiple sclerosis. *Front Neurosci* **9**, 264 (2015).
32. J. Bruna, R. Velasco, Sigma-1 receptor: a new player in neuroprotection against chemotherapy-induced peripheral neuropathy. *Neural Regen Res* **13**, 775-778 (2018).
33. L. Romero, M. Merlos, J. M. Vela, Antinociception by Sigma-1 Receptor Antagonists: Central and Peripheral Effects. *Adv Pharmacol* **75**, 179-215 (2016).
34. L. Romero *et al.*, Pharmacological properties of S1RA, a new sigma-1 receptor antagonist that inhibits neuropathic pain and activity-induced spinal sensitization. *Br J Pharmacol* **166**, 2289-2306 (2012).
35. B. de la Puente *et al.*, Sigma-1 receptors regulate activity-induced spinal sensitization and neuropathic pain after peripheral nerve injury. *Pain* **145**, 294-303 (2009).
36. D. Tavares-Ferreira *et al.*, Spatial transcriptomics of dorsal root ganglia identifies molecular signatures of human nociceptors. *Sci Transl Med* **14**, eabj8186 (2022).
37. D. Usoskin *et al.*, Unbiased classification of sensory neuron types by large-scale single-cell RNA sequencing. *Nat Neurosci* **18**, 145-153 (2015).
38. J. J. Sahn, T. R. Hodges, J. Z. Chan, S. F. Martin, Norbenzomorphan Scaffold: Chemical Tool for Modulating Sigma Receptor-Subtype Selectivity. *ACS Med Chem Lett* **8**, 455-460 (2017).
39. S. F. Martin, Bridging Known and Unknown Unknowns: From Natural Products and Their Mimics to Unmet Needs in Neuroscience. *Accounts of Chemical Research* **55**, 2397-2408 (2022).
40. M. Hanner *et al.*, Purification, molecular cloning, and expression of the mammalian sigma1-binding site. *Proc Natl Acad Sci U S A* **93**, 8072-8077 (1996).
41. D. E. Gordon *et al.*, A SARS-CoV-2 protein interaction map reveals targets for drug repurposing. *Nature* **583**, 459-468 (2020).
42. K. E. Inyang *et al.*, Indirect AMP-Activated Protein Kinase Activators Prevent Incision-Induced Hyperalgesia and Block Hyperalgesic Priming, Whereas Positive Allosteric Modulators Block Only Priming in Mice. *J Pharmacol Exp Ther* **371**, 138-150 (2019).
43. K. E. Inyang *et al.*, The antidiabetic drug metformin prevents and reverses neuropathic pain and spinal cord microglial activation in male but not female mice. *Pharmacol Res* **139**, 1-16 (2019).
44. K. E. Inyang *et al.*, Alleviation of paclitaxel-induced mechanical hypersensitivity and hyperalgesic priming with AMPK activators in male and female mice. *Neurobiol Pain* **6**, 100037 (2019).
45. M. D. Burton *et al.*, Pharmacological activation of AMPK inhibits incision-evoked mechanical hypersensitivity and the development of hyperalgesic priming in mice. *Neuroscience* **359**, 119-129 (2017).
46. A. Bertolotti, Y. Zhang, L. M. Hendershot, H. P. Harding, D. Ron, Dynamic interaction of BiP and ER stress transducers in the unfolded-protein response. *Nat Cell Biol* **2**, 326-332 (2000).
47. A. A. Anand, P. Walter, Structural insights into ISRIB, a memory-enhancing inhibitor of the integrated stress response. *FEBS J* **287**, 239-245 (2020).
48. Uhl *et al.*, Tissue-based map of the human proteome. *Science* **347**, 394-394 (2015).
49. L. L. Scott *et al.*, Small molecule modulators of sigma2R/Tmem97 reduce alcohol withdrawal-induced behaviors. *Neuropsychopharmacology* **43**, 1867-1875 (2018).

50. S. G. Quadir *et al.*, The Sigma-2 receptor / transmembrane protein 97 (sigma2R/TMEM97) modulator JVW-1034 reduces heavy alcohol drinking and associated pain states in male mice. *Neuropharmacology* **184**, 108409 (2021).
51. S. Mondal *et al.*, High-Content Microfluidic Screening Platform Used To Identify sigma2R/Tmem97 Binding Ligands that Reduce Age-Dependent Neurodegeneration in C. elegans SC_APP Model. *ACS Chem Neurosci* **9**, 1014-1026 (2018).
52. Y. Li *et al.*, A011, a novel small-molecule ligand of sigma2 receptor, potently suppresses breast cancer progression via endoplasmic reticulum stress and autophagy. *Biomed Pharmacother* **152**, 113232 (2022).
53. B. F. Teske *et al.*, The eIF2 kinase PERK and the integrated stress response facilitate activation of ATF6 during endoplasmic reticulum stress. *Molecular Biology of the Cell* **22**, 4390-4405 (2011).
54. U. I. Onat *et al.*, Intercepting the Lipid-Induced Integrated Stress Response Reduces Atherosclerosis. *J Am Coll Cardiol* **73**, 1149-1169 (2019).
55. M. J. Jennings *et al.*, Intracellular Lipid Accumulation and Mitochondrial Dysfunction Accompanies Endoplasmic Reticulum Stress Caused by Loss of the Co-chaperone DNAJC3. *Front Cell Dev Biol* **9**, 710247 (2021).
56. M. S. Yousuf, A. D. Maguire, T. Simmen, B. J. Kerr, Endoplasmic reticulum-mitochondria interplay in chronic pain: The calcium connection. *Mol Pain* **16**, 1744806920946889 (2020).
57. S. P. Sherman, A. G. Bang, High-throughput screen for compounds that modulate neurite growth of human induced pluripotent stem cell derived neurons. *Disease Models & Mechanisms* **11**, dmm031906 (2018).
58. S. K. Young-Baird *et al.*, Suppression of MEHMO Syndrome Mutation in eIF2 by Small Molecule ISRIB. *Molecular Cell* **77**, 875-886.e877 (2020).
59. L. M. Mangus, D. B. Rao, G. J. Ebenezer, Intraepidermal Nerve Fiber Analysis in Human Patients and Animal Models of Peripheral Neuropathy: A Comparative Review. *Toxicologic Pathology* **48**, 59-70 (2020).
60. A. Khoutorsky *et al.*, eIF2alpha phosphorylation controls thermal nociception. *Proc Natl Acad Sci U S A* **113**, 11949-11954 (2016).
61. R. P. Bonin, C. Bories, Y. De Koninck, A Simplified Up-Down Method (SUDO) for Measuring Mechanical Nociception in Rodents Using von Frey Filaments. *Molecular Pain* **10**, 1744-8069-1710-1726 (2014).
62. K. Hargreaves, R. Dubner, F. Brown, C. Flores, J. Joris, A new and sensitive method for measuring thermal nociception in cutaneous hyperalgesia. *Pain* **32**, 77-88 (1988).
63. M. V. Valtcheva *et al.*, Surgical extraction of human dorsal root ganglia from organ donors and preparation of primary sensory neuron cultures. *Nat Protoc* **11**, 1877-1888 (2016).
64. S. I. Shiers *et al.*, Convergence of peptidergic and non-peptidergic protein markers in the human dorsal root ganglion and spinal dorsal horn. *J Comp Neurol* **529**, 2771-2788 (2021).
65. M. S. Yousuf *et al.*, Sensory Neurons of the Dorsal Root Ganglia Become Hyperexcitable in a T-Cell-Mediated MOG-EAE Model of Multiple Sclerosis. *eNeuro* **6** (2019).
66. C. R. Eddings *et al.*, Pridopidine protects neurons from mutant-huntingtin toxicity via the sigma-1 receptor. *Neurobiol Dis* **129**, 118-129 (2019).
67. T. A. Ferreira *et al.*, Neuronal morphometry directly from bitmap images. *Nature Methods* **11**, 982-984 (2014).
68. J. Besnard *et al.*, Automated design of ligands to polypharmacological profiles. *Nature* **492**, 215-220 (2012).

69. S. Megat *et al.*, Nociceptor Translational Profiling Reveals the Ragulator-Rag GTPase Complex as a Critical Generator of Neuropathic Pain. *J Neurosci* **39**, 393-411 (2019).
70. J. J. Sahn, S. F. Martin, Expedient synthesis of norbenzomorphan library via multicomponent assembly process coupled with ring-closing reactions. *ACS Comb Sci* **14**, 496-502 (2012).

Figures and Figure Legends

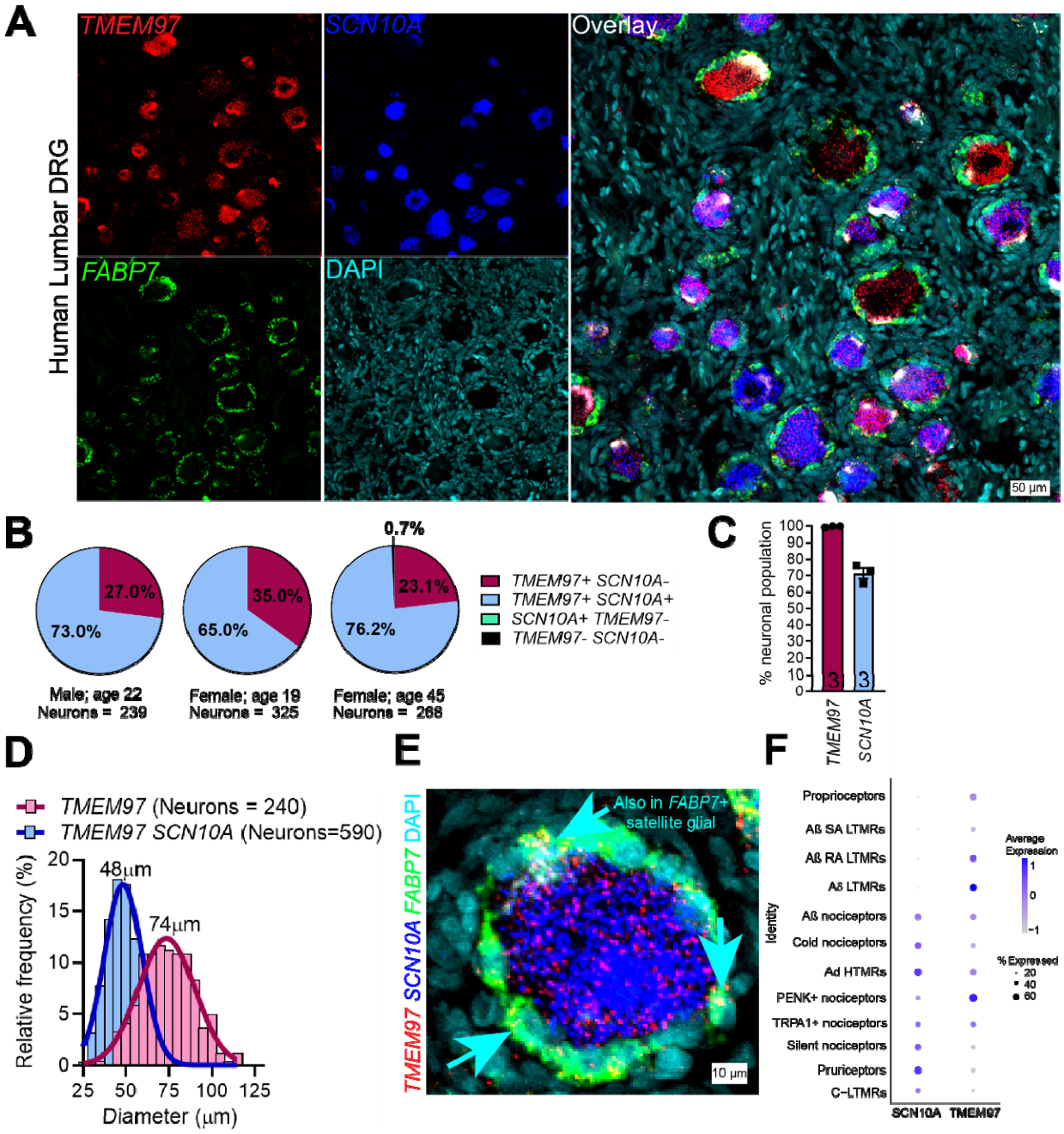

Figure 1. *TMEM97* gene is expressed in human dorsal root ganglia (DRG). (A) RNAScope *in situ* hybridization experiments using lumbar DRGs obtained from organ donors. (B-C) Across 3 donors (1 male and 2 females), we discovered that nearly all DRG neurons (>99%) expressed *TMEM97* and notably, all *SCN10A*-positive nociceptors expressed *TMEM97*. (D) *TMEM97*-positive neurons were distributed across all cell sizes. (E) Upon further investigation, we also identified *TMEM97* transcripts in *FABP7*-positive satellite glial cells. (F) Our previously published (36) analysis of near single-cell RNA sequencing of human DRGs showed that *TMEM97* is expressed across all neuronal cell types in the ganglia including nociceptors, low-threshold mechanoreceptors (LTMRs), and proprioceptors.

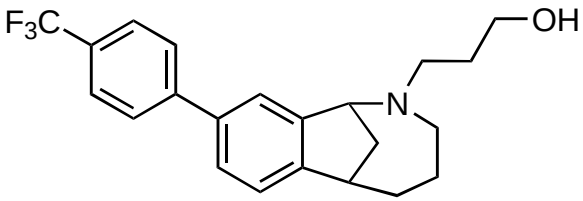

UKH-1114

σ_2R/TMEM97 K_i (nM): 46

σ1R K_i (nM): 1279

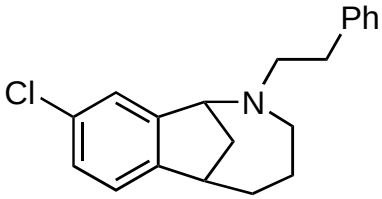

JVW-1034

σ_2R/TMEM97 K_i (nM): 23

σ_1R K_i (nM): 248

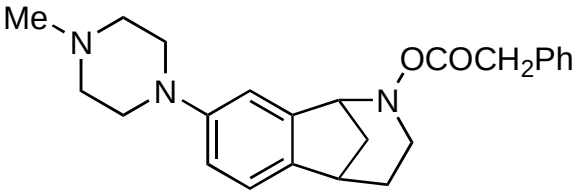

SAS-0132

σ_2R/TMEM97 K_i (nM): 90

σ_1R K_i (nM): 841

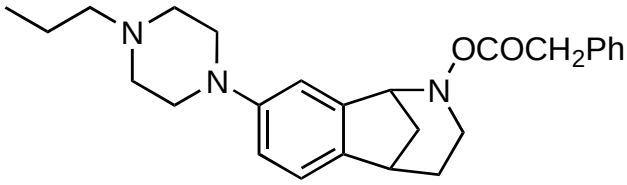

DKR-1677

σ_2R/TMEM97 K_i (nM): 5.1

σ_1R K_i (nM): 230

Figure 2. Structures and binding affinities of selected biologically-active methanobenzazocines (e.g. UKH-1114 and JVW-1034) and norbenzomorphans (e.g. SAS-0132 and DKR-1677). K_i values were determined at the PDSP using σ_2R/TMEM97 sourced from rat PC12 cells and σ_1R sourced from guinea pig brain, and values are reported as an average of two or more independent experiments (68).

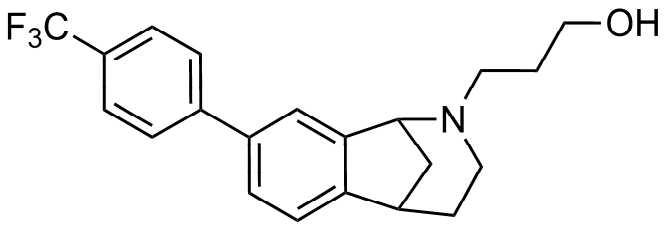

FEM-1689

σ_2R/TMEM97 K_i (nM): 11

Highly selective

>100-fold selective for more than 40 CNS proteins except for:

19-fold vs σ_1R (206 nM)

37-fold vs NET (404 nM)

Physicochemical properties

MW	361
CLogP	4.4
tPSA	23.5 Å^2
H-bond donors	1
H-bond acceptors	2
Rotatable bonds	5

PK properties and brain exposure

T_{max} (IP): 0.5 h (plasma); 2 h (brain)

C_{max} (IP): 508 ng/mL (plasma); 10916 ng/mL (brain)

$t_{1/2}$ (IP): 21.7 h (plasma); 11.4 (brain)

brain to plasma ratio (AUC_{last}): 20.5

Figure 3. Structure, binding profiles, physicochemical properties, and pharmacokinetic parameters for FEM-1689.

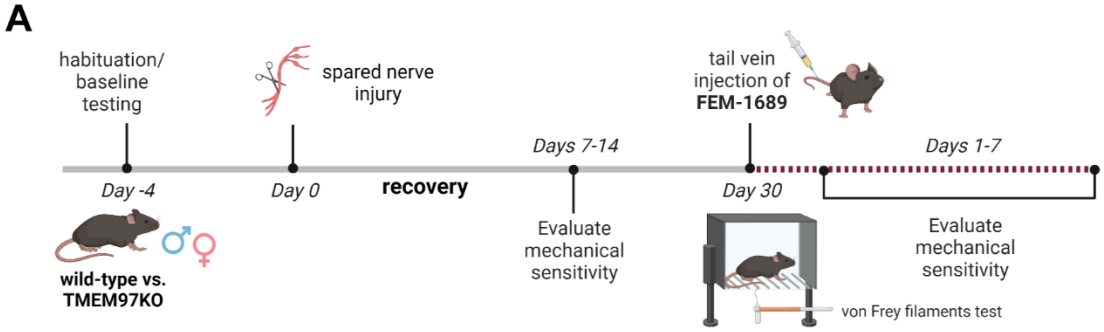

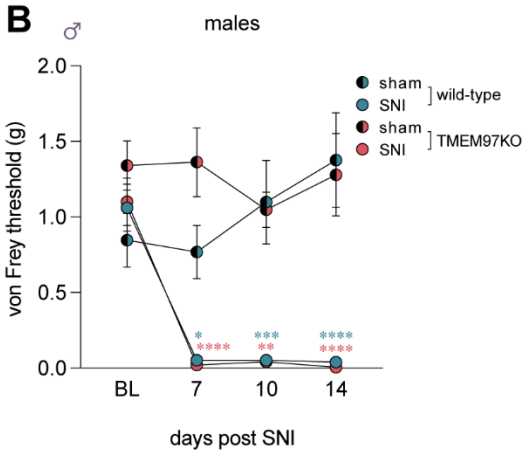

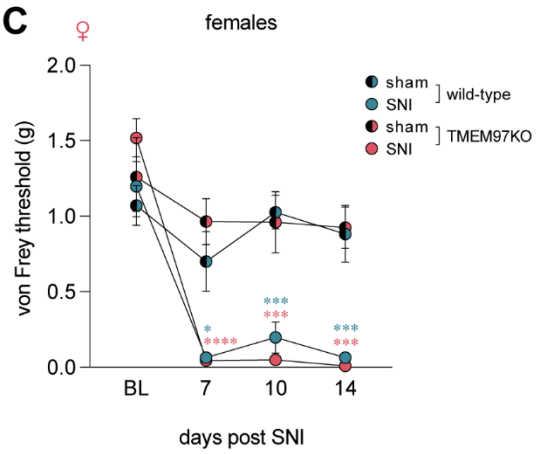

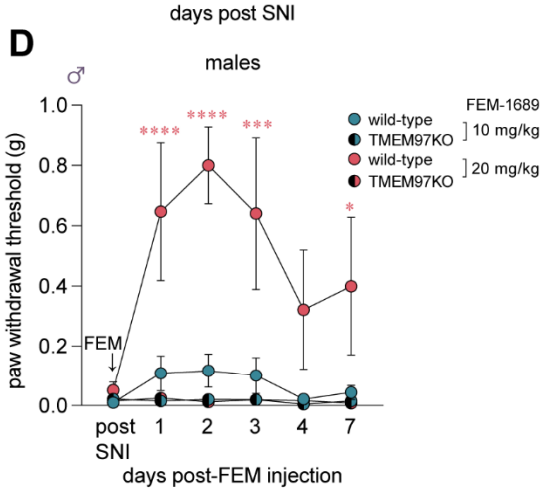

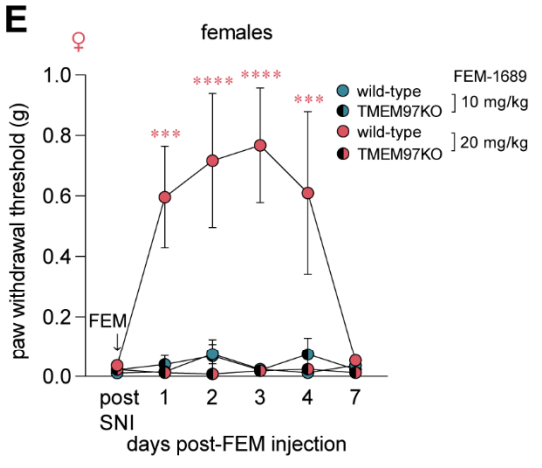

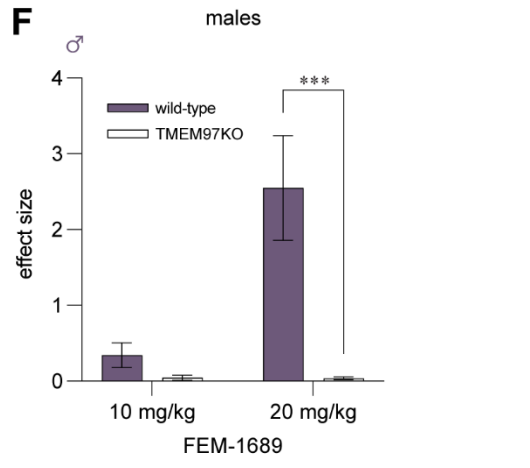

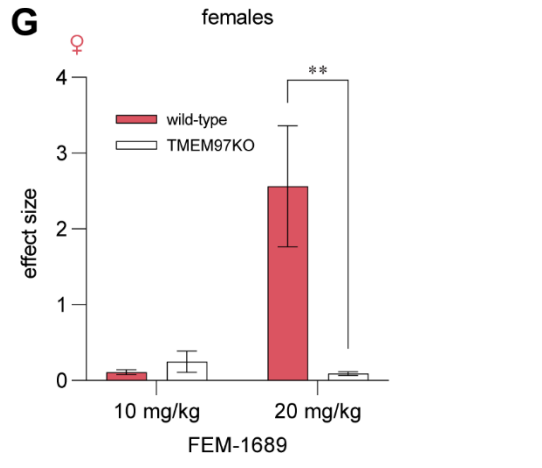

Figure 4. Mechanical pain hypersensitivity following spared nerve injury in wild-type and global TMEM97-knockout (KO) mice. (A) Experimental paradigm. Mechanical pain hypersensitivity was assessed using the von Frey filaments test at baseline prior to spared nerve injury (SNI) and for 14 days post-surgery. Mice were treated with FEM-1689 (10 mg/kg) intravenously thirty (30) days after SNI surgery and assessed for mechanical hypersensitivity for the following 7 days. Another intravenous injection of FEM-1689 (20 mg/kg) was given 2 weeks later and mechanical hypersensitivity assessed for 7 days. (B, C) Following SNI, no significant difference in mechanical hypersensitivity between wild-type and TMEM97KO littermates of both sexes was observed, suggesting that TMEM97 did not contribute to the development of neuropathic pain following nerve injury. Wild-type SNI (male n=6, female n=5), wild-type sham (male n=6, female n=5), TMEM97KO SNI (male n=5, female n=5), TMEM97KO sham (male n=5, female n=5). (D, E) A single 20 mg/kg intravenous injection of FEM-1689 reversed mechanical hypersensitivity in wild-type (male n=6, female n=5) but not TMEM97KO (male n=5, female n=5) mice. A lower dose of 10 mg/kg was not sufficient to reduce mechanical hypersensitivity in these animals. Repeated measures two-way ANOVA with Holm-Sidak's multiple comparison test, *p<0.05, **p<0.01, ***p<0.001, ****p<0.0001. (F, G) Effect size analysis demonstrates that a higher dose of 20 mg/kg of FEM-1689 provides maximal analgesic effect. Two-way ANOVA with Sidak's multiple comparison test, **p<0.01, ***p<0.001. Blue and red asterisks indicate wild-type and TMEM97KO groups compared to sham controls in (B, C) and wild-type vs. TMEM97KO groups in (D, E).

.

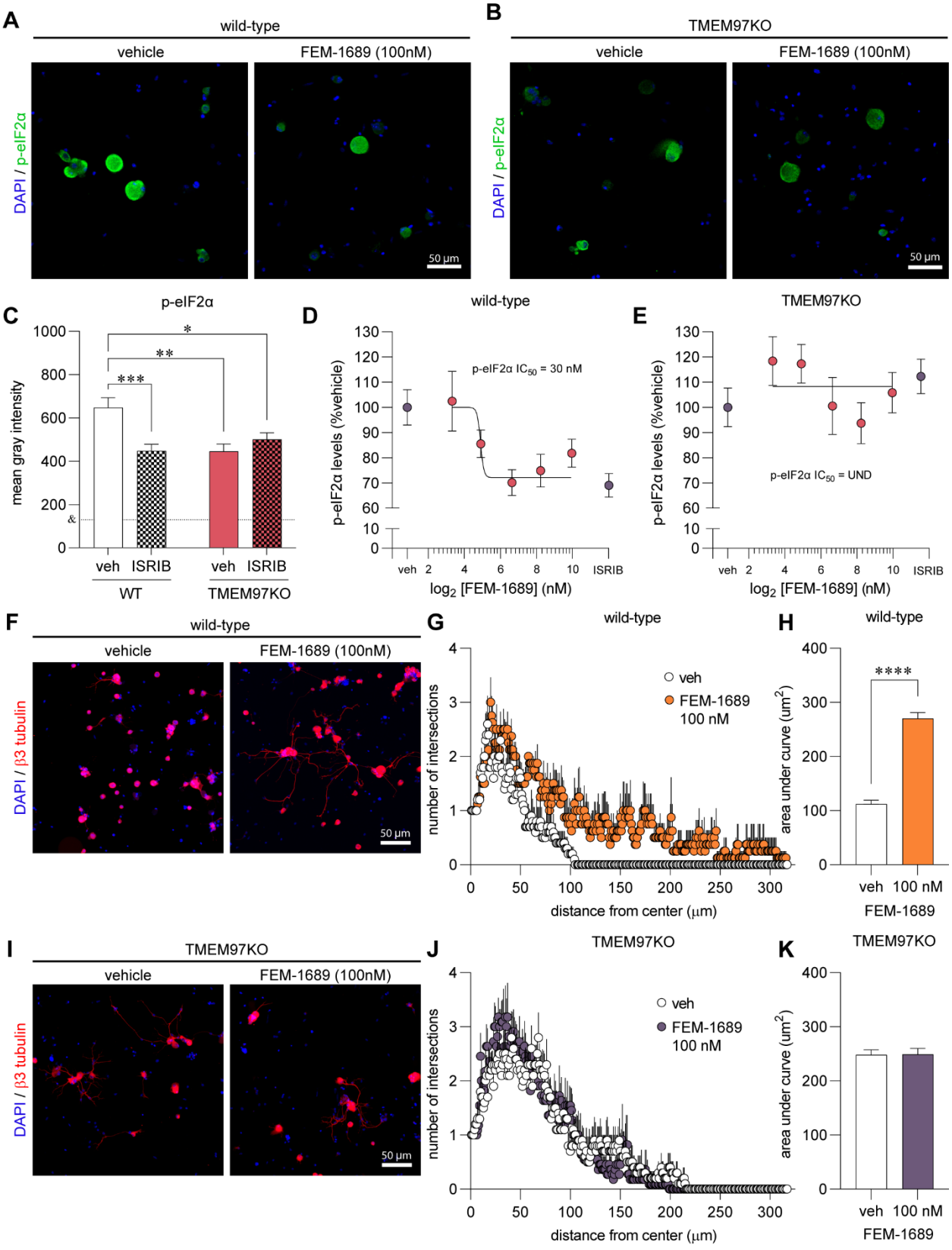

Figure 5. FEM-1689 reduced p-eIF2α levels and promoted neurite outgrowth *in vitro*. (A, B) Cultured mouse DRG neurons obtained from wild-type and TMEM97KO animals were treated with FEM-1689 over 16 hours. Basal levels of p-eIF2α were lower in TMEM97KO neurons. ISRIB (200 nM) reduced p-eIF2α levels in wild-type neurons but failed to change p-eIF2α immunoreactivity in TMEM97KO neurons (C). Immunoreactivity of p-eIF2α was assessed and a 9-point dose-response curve ranging from 0.1 nM to 1000 nM was generated as a percentage of p-eIF2α levels of vehicle treated cells. An IC_{50} of 30 nM was determined with maximal effect at 100 nM which was comparable to ISRIB (200 nM) treatment (D, E). TMEM97KO DRG neurons did not respond to FEM-1689 treatment. (F-K) Sholl analysis of mouse DRG neurons following 100 nM of FEM-1689 treatment showed an increase in the number and complexity of neurites in wild-type neurons but not in TMEM97KO neurons. Area under the curve of Sholl analysis was used to statistically demonstrate this effect. Immunoreactivity against β3-tubulin was used to identify neuronal cell bodies and neurites. ***p<0.001, ****p<0.0001 two-tailed Student's t-test. UND=undetermined. &=average mean gray intensity of the primary omission control.

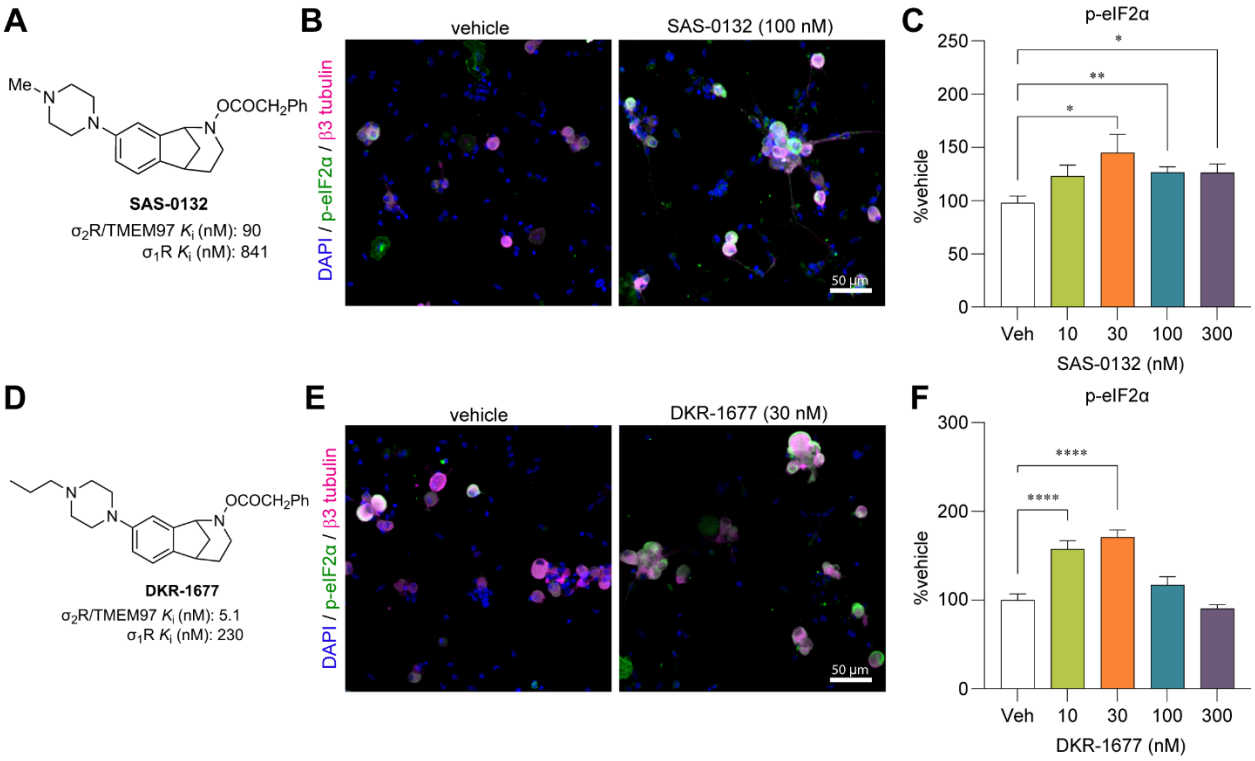

Figure 6. Norbenzomorphans such as SAS-0132 (A-C) and DKR-1677 (D-F) stimulate the ISR by promoting the phosphorylation of eIF2α in cultured wild-type mouse DRG neurons. Cells were treated for 16 hours with either SAS-0132 or DKR-1677 at 10, 30, 100, or 300nM concentrations. Data is presented as fold-change compared to the fluorescence measured in the vehicle treated neurons. *p<0.05, **p<0.01, ****p<0.0001 One-way ANOVA with Tukey's post hoc test.

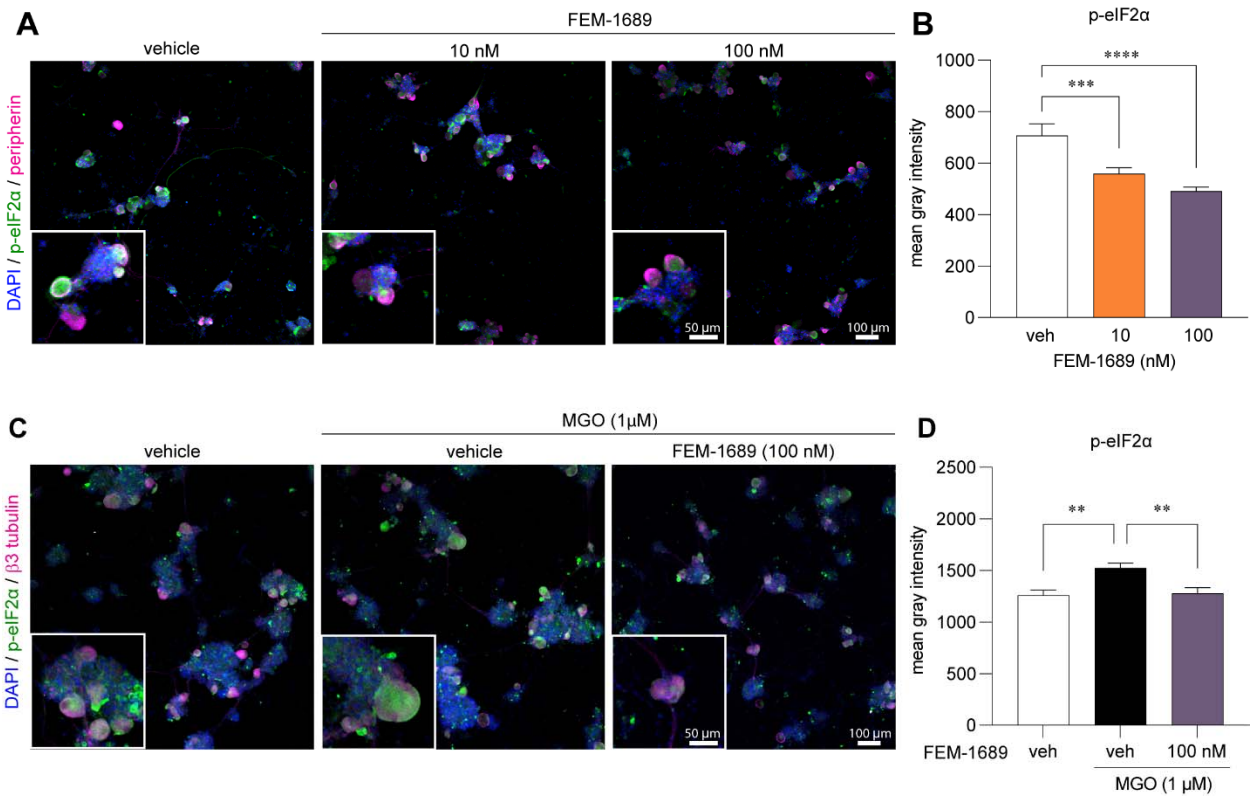

Figure 7. (A, B) FEM-1689 treatment (10 and 100nM) of cultured human DRG neurons significantly reduced p-eIF2α levels. (C, D) Methylglyoxal (MGO) is known to induce the ISR. Co-treatment of human neurons with MGO (1 µM) and FEM-1689 (100 nM) prevented an increase in p-eIF2α suggesting that FEM-1689 limits the effect of MGO. Peripherin and β3-tubulin were used to identify neurons. One-way ANOVA followed by Tukey's post-hoc test **p<0.01, ***p<0.001, ****p<0.0001.

Figure 1

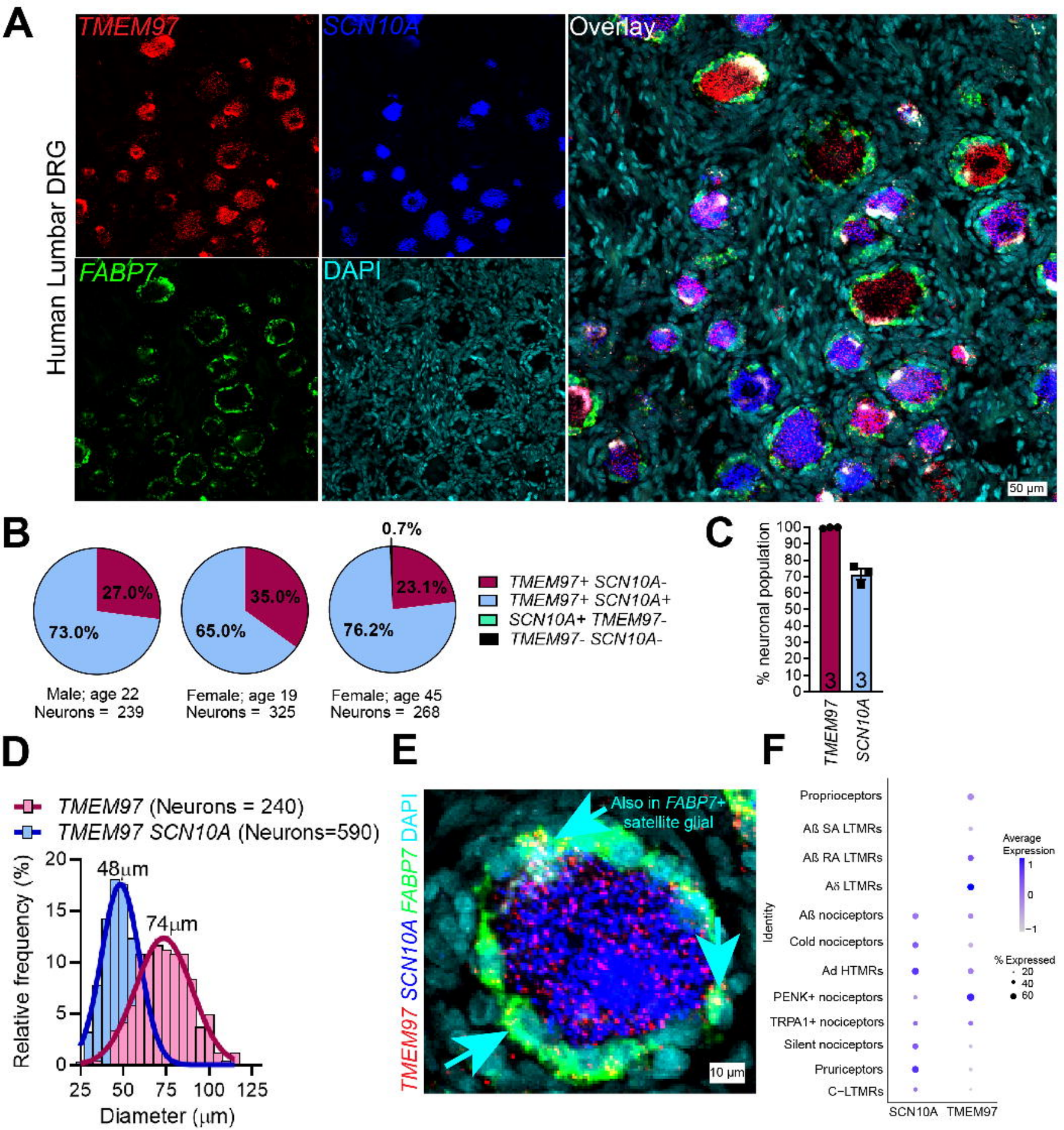
A
TMEM97
SCN10A
Overlay
FABP7
DAPI
Human Lumbar DRG
50 µm
B
27.0%
73.0%
35.0%
65.0%
0.7%
23.1%
76.2%
Male; age 22
Neurons = 239
Female; age 19
Neurons = 325
Female; age 45
Neurons = 268
TMEM97+ SCN10A-
TMEM97+ SCN10A+
SCN10A+ TMEM97-
TMEM97- SCN10A-
C
% neuronal population
100
90
80
70
60
50
40
30
20
10
0
3
3
TMEM97
SCN10A
D
TMEM97 (Neurons = 240)
TMEM97 SCN10A (Neurons=590)
Relative frequency (%)
20
15
10
5
0
48µm
74µm
25
50
75
100
125
Diameter (µm)
E
TMEM97 SCN10A FABP7 DAPI
Also in FABP7+
satellite glial
10 µm
F
Proprioceptors
Aß SA LTMRs
Aß RA LTMRs
Aδ LTMRs
Aß nociceptors
Cold nociceptors
Ad HTMRs
PENK+ nociceptors
TRPA1+ nociceptors
Silent nociceptors
Pruriceptors
C-LTMRs
Identity
SCN10A
TMEM97
Average
Expression
1
0
-1
% Expressed
20
40
60

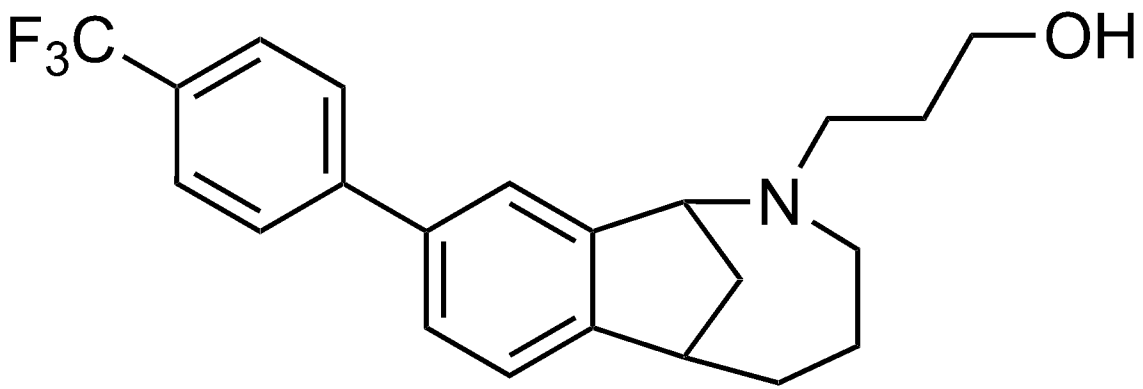

UKH-1114

σ_2R/TMEM97 K_i (nM): 46

σ1R K_i (nM): 1279

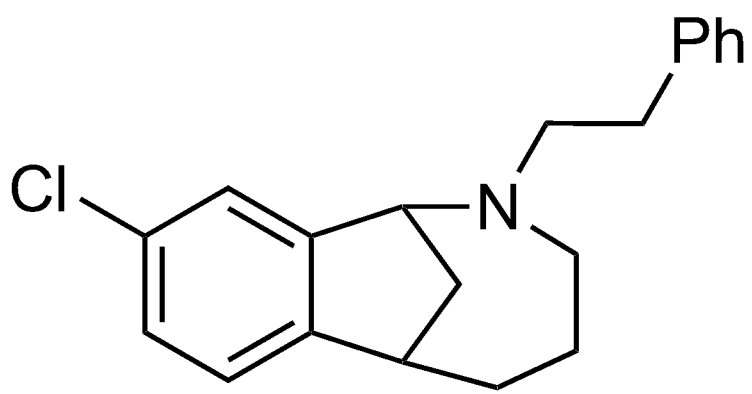

JVW-1034

σ_2R/TMEM97 K_i (nM): 23

σ_1R K_i (nM): 248

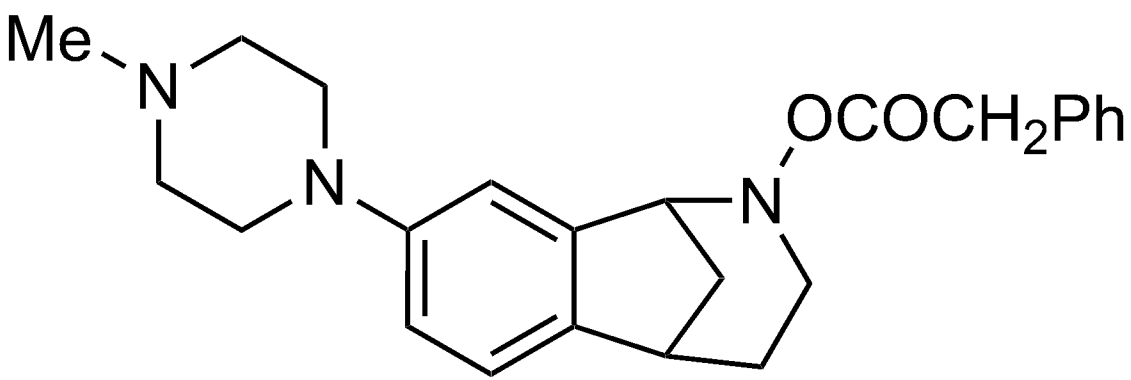

SAS-0132

σ_2R/TMEM97 K_i (nM): 90

σ_1R K_i (nM): 841

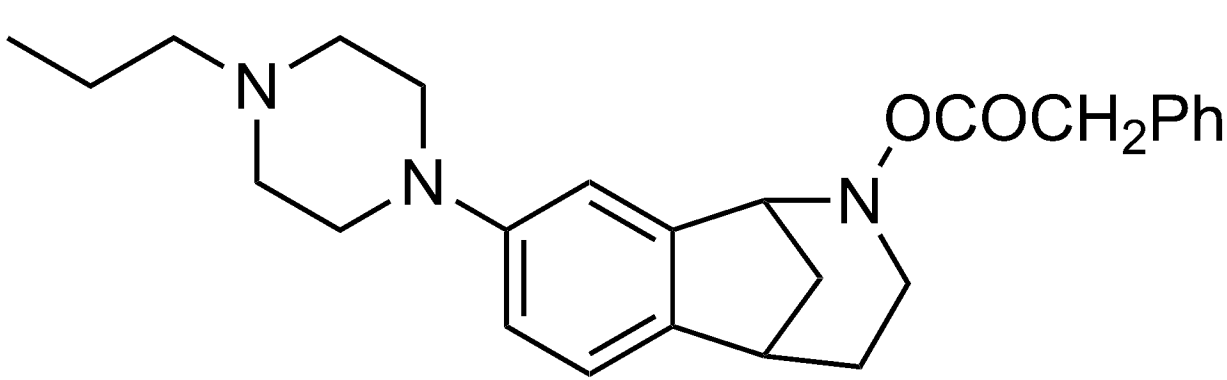

DKR-1677

σ_2R/TMEM97 K_i (nM): 5.1

σ_1R K_i (nM): 230

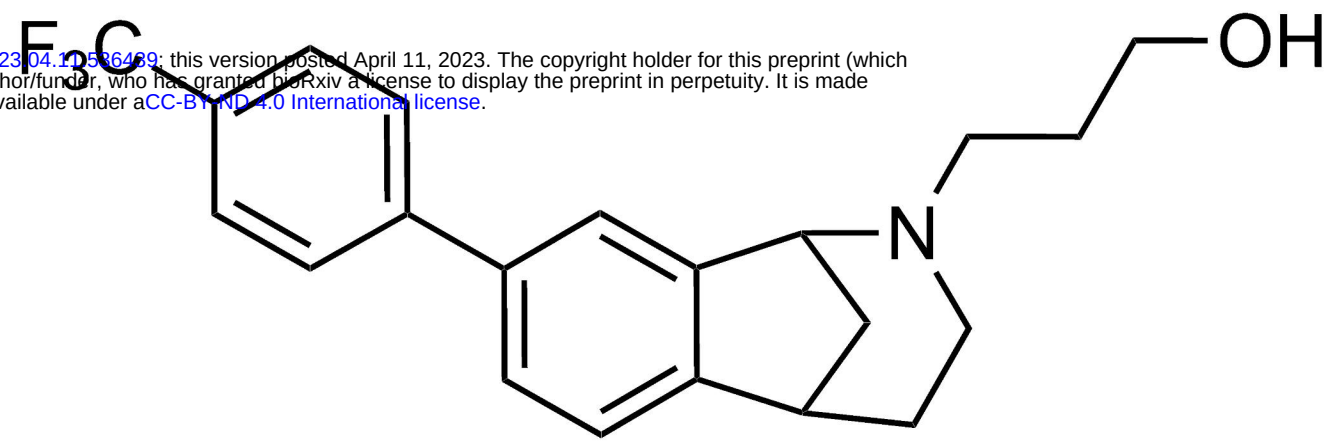

FEM-1689

σ_2R/TMEM97 K_i (nM): 11

Highly selective

>100-fold selective for more than 40 CNS proteins except for:

19-fold vs σ_1R (206 nM)

37-fold vs NET (404 nM)

Physicochemical properties

MW	361
CLogP	4.4
tPSA	23.5 Å^2
H-bond donors	1
H-bond acceptors	2
Rotatable bonds	5

PK properties and brain exposure

T_{max} (IP): 0.5 h (plasma); 2 h (brain)

C_{max} (IP): 508 ng/mL (plasma);
10916 ng/mL (brain)

$t_{1/2}$ (IP): 21.7 h (plasma); 11.4 (brain)

brain to plasma ratio (AUC_{last}): 20.5

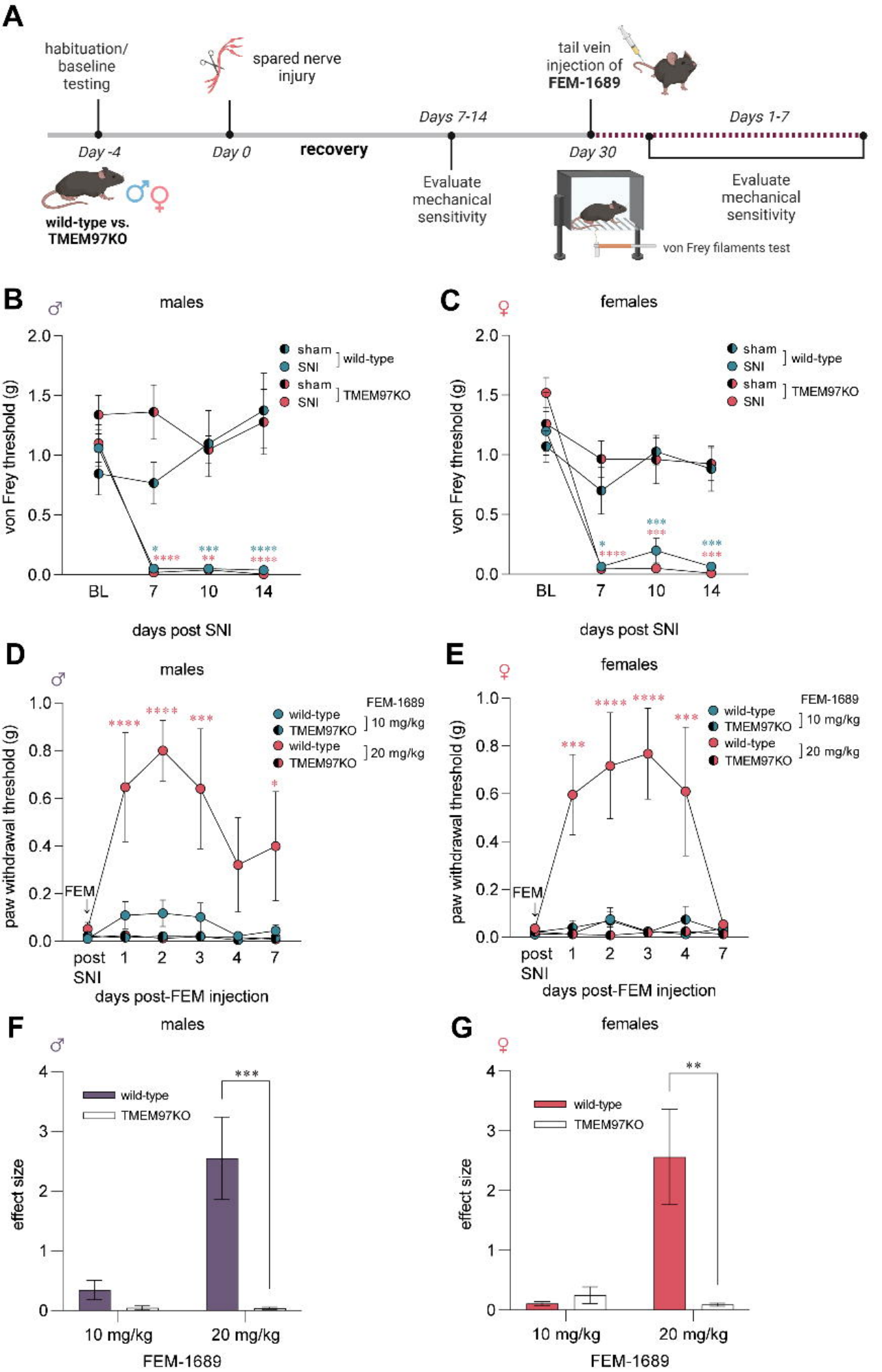
A
habituation/
baseline
testing
spared nerve
injury
tail vein
injection of
FEM-1689
Days 7-14
Days 1-7
Day -4
Day 0
recovery
Day 30
Evaluate
mechanical
sensitivity
Evaluate
mechanical
sensitivity
wild-type vs.
TMEM97KO
von Frey filaments test
B
males
C
females
sham
SNI
wild-type
sham
SNI
TMEM97KO
von Frey threshold (g)
BL
7
10
14
days post SNI
D
males
E
females
FEM-1689
wild-type
TMEM97KO
10 mg/kg
20 mg/kg
paw withdrawal threshold (g)
FEM
post
SNI
1
2
3
4
7
days post-FEM injection
F
males
G
females
wild-type
TMEM97KO
effect size
10 mg/kg
20 mg/kg
FEM-1689

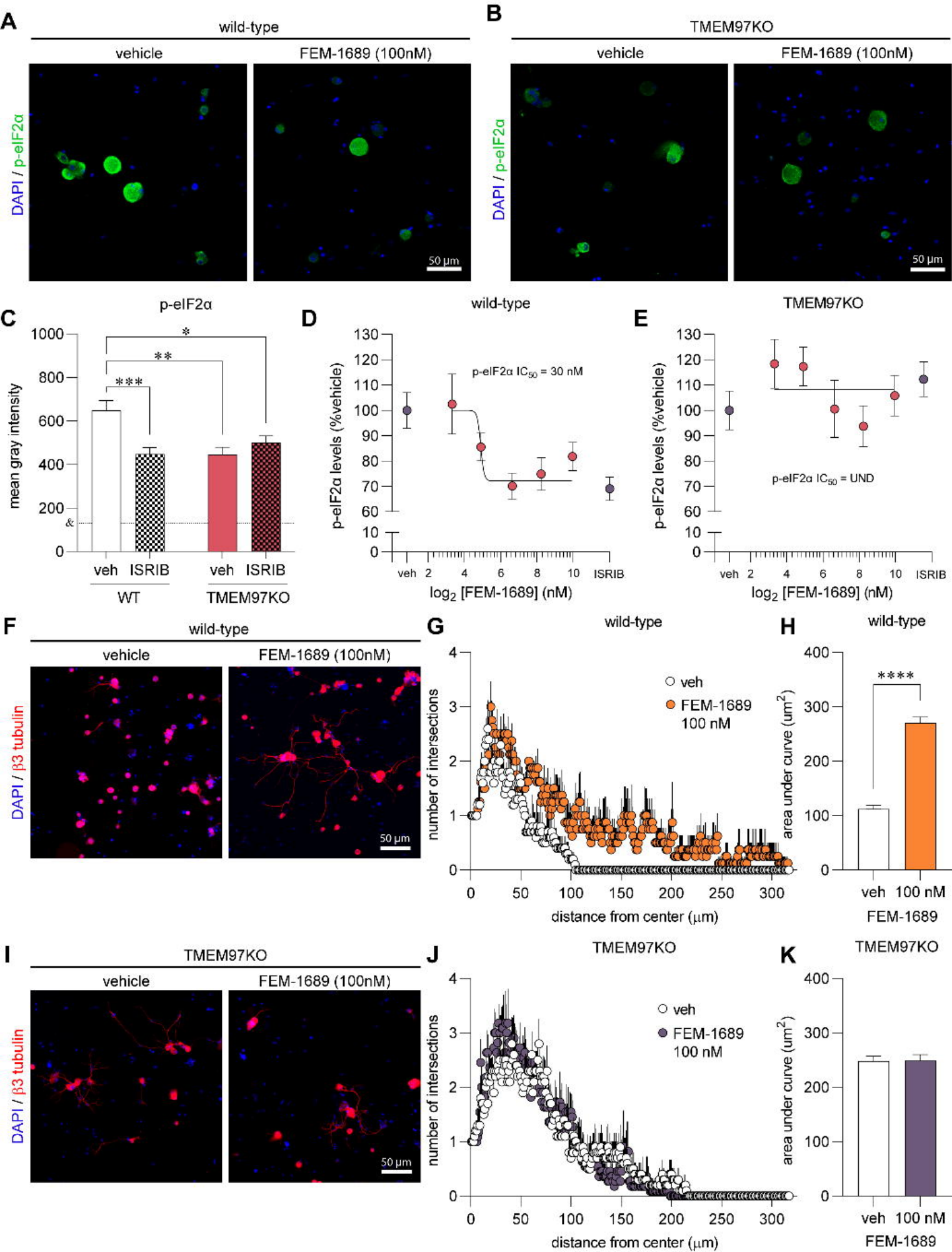
A
wild-type
vehicle
FEM-1689 (100nM)
DAPI / p-eIF2α
50 µm
B
TMEM97KO
vehicle
FEM-1689 (100nM)
DAPI / p-eIF2α
50 µm
C
p-eIF2α
mean gray intensity
1000
800
600
400
200
0
&
*
**
***
veh
ISRIB
veh
ISRIB
WT
TMEM97KO
D
wild-type
p-eIF2α levels (%vehicle)
p-eIF2α IC50 = 30 nM
log2 [FEM-1689] (nM)
veh
ISRIB
E
TMEM97KO
p-eIF2α levels (%vehicle)
p-eIF2α IC50 = UND
log2 [FEM-1689] (nM)
veh
ISRIB
F
wild-type
vehicle
FEM-1689 (100nM)
DAPI / β3 tubulin
50 µm
G
wild-type
number of intersections
veh
FEM-1689
100 nM
distance from center (µm)
H
wild-type
area under curve (um2)
****
veh
100 nM
FEM-1689
I
TMEM97KO
vehicle
FEM-1689 (100nM)
DAPI / β3 tubulin
50 µm
J
TMEM97KO
number of intersections
veh
FEM-1689
100 nM
distance from center (µm)
K
TMEM97KO
area under curve (um2)
veh
100 nM
FEM-1689

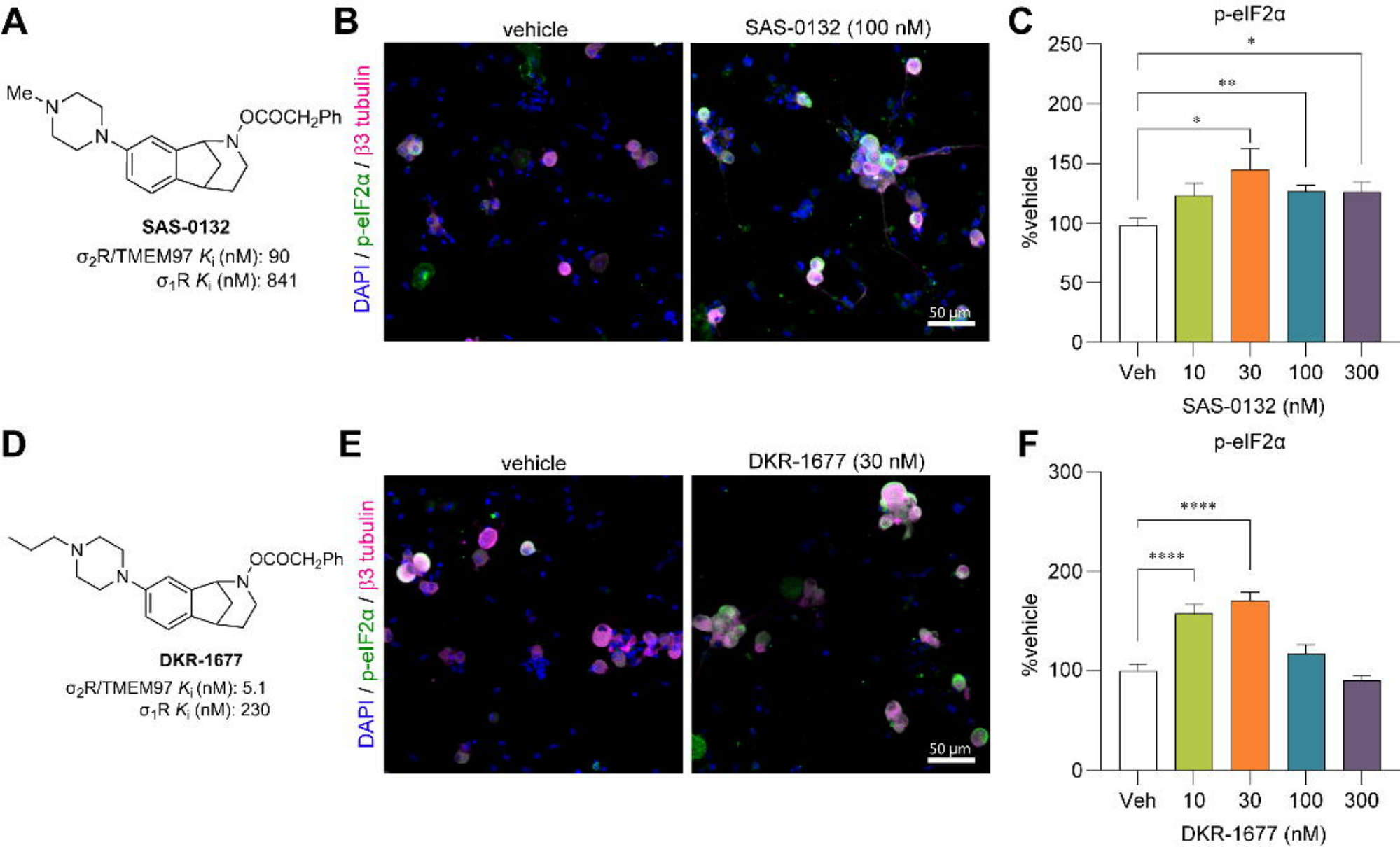
A
Me
N
N
N
OCOCH2Ph
SAS-0132
σ2R/TMEM97 Ki (nM): 90
σ1R Ki (nM): 841
B
vehicle
SAS-0132 (100 nM)
DAPI / p-eIF2α / β3 tubulin
50 μm
C
p-eIF2α
%vehicle
250
200
150
100
50
0
*
**
*
Veh
10
30
100
300
SAS-0132 (nM)
D
N
N
N
OCOCH2Ph
DKR-1677
σ2R/TMEM97 Ki (nM): 5.1
σ1R Ki (nM): 230
E
vehicle
DKR-1677 (30 nM)
DAPI / p-eIF2α / β3 tubulin
50 μm
F
p-eIF2α
%vehicle
300
200
100
0
****
****
Veh
10
30
100
300
DKR-1677 (nM)

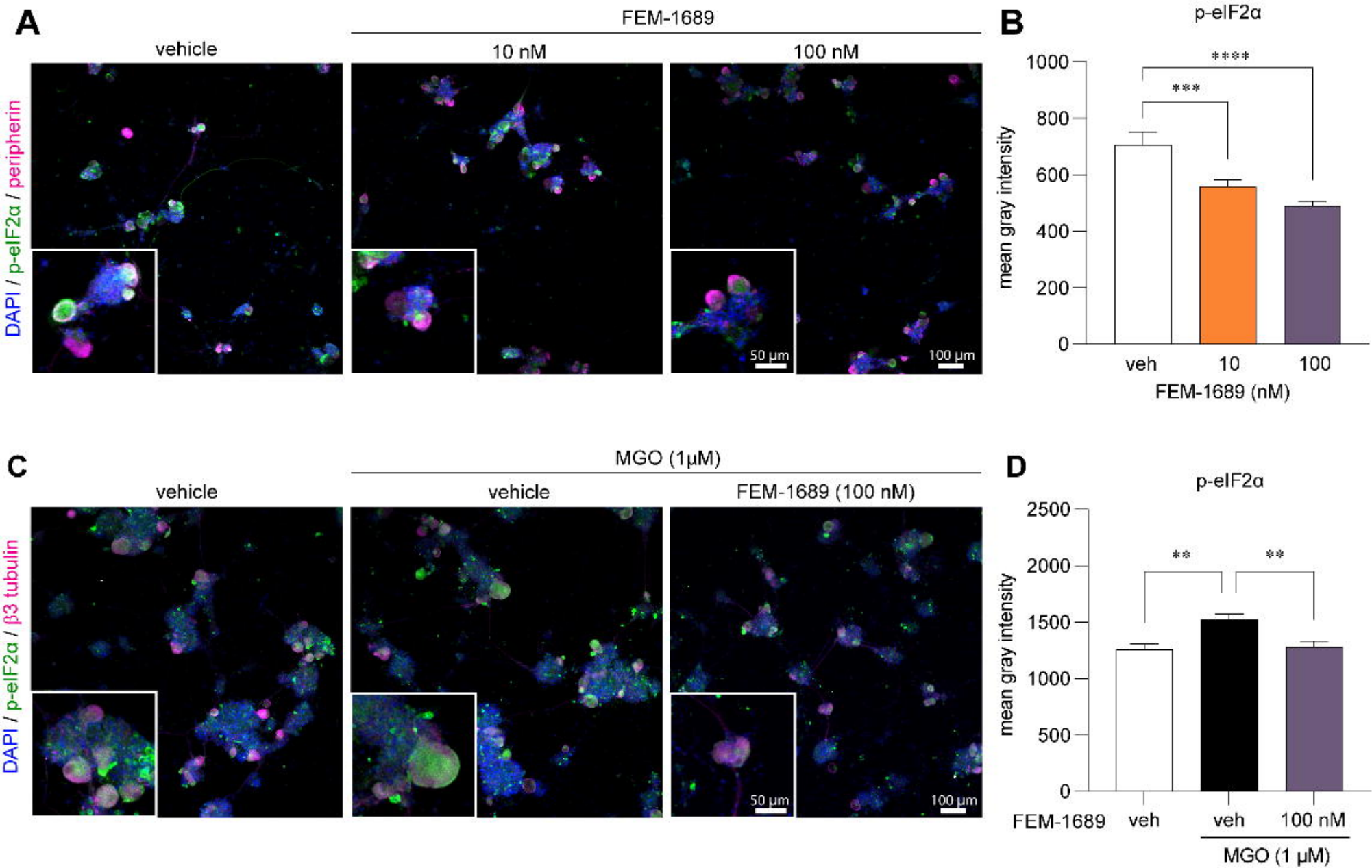
A
FEM-1689
vehicle
10 nM
100 nM
DAPI / p-eIF2α / peripherin
50 µm
100 µm
B
p-eIF2α
mean gray intensity
1000
800
600
400
200
0
****
***
veh
10
100
FEM-1689 (nM)
C
MGO (1µM)
vehicle
vehicle
FEM-1689 (100 nM)
DAPI / p-eIF2α / β3 tubulin
50 µm
100 µm
D
p-eIF2α
mean gray intensity
2500
2000
1500
1000
500
0
**
**
FEM-1689
veh
veh
100 nM
MGO (1 µM)